ANTHROPOLOGY

Pre-Clovis projectile points at the Debra L. Friedkin site, Texas—Implications for the Late Pleistocene peopling of the Americas

Michael R. Waters[1,2*†], Joshua L. Keene[1,2†], Steven L. Forman[3], Elton R. Prewitt[4], David L. Carlson[2], James E. Wiederhold[1]

Lanceolate projectile points of the Clovis complex and stemmed projectile points of the Western Stemmed Tradition first appeared in North America by ~13 thousand years (ka) ago. The origin, age, and chronological superposition of these stemmed and lanceolate traditions are unclear. At the Debra L. Friedkin site, Texas, below Folsom and Clovis horizons, we find stemmed projectile points dating from ~13.5 to ~15.5 ka ago, with a triangular lanceolate point form appearing ~14 ka ago. The sequential relationship of stemmed projectile points followed by lanceolate forms suggests that lanceolate points are derived from stemmed forms or that they originated from two separate migrations into the Americas.

INTRODUCTION

Our understanding of the process of the peopling of the Americas is undergoing rapid change with new archaeological and genetic discoveries. For decades, it was believed that the first people entered the Americas ~13.5 thousand years (ka) ago via an ice-free corridor, developed the distinctive Clovis tool kit with its iconic, fluted, lanceolate projectile point, and then rapidly spread across North America, with their descendants eventually reaching South America ~12.9 ka ago. However, over the past decade, genetic studies of modern Native Americans and prehistoric skeletons have shown that the initial movement of people south of the continental ice sheets occurred as early as ~15 to ~16 ka ago and that there is genetic continuity between the first immigrants to enter the Americas and modern Native Americans (*1*, *2*). Archaeological studies over the last 25 years show that people successfully occupied the Americas ~14 to ~15 ka ago, in agreement with the genetic estimates. In South America, humans occupied Monte Verde, Chile, by ~14.2 ka ago (*3*), indicating that people must have been in North America ≥14.2 ka ago. In North America, humans were present during the period ~14 to ~15 ka ago, as documented by archaeological evidence radiocarbon dated to ~14.6 ka ago at Page-Ladson, Florida (*4*); ~14.2 ka ago at Paisley Caves, Oregon (*5*); ~14.2 and ~14.8 ka ago at Schaefer and Hebior, Wisconsin (*6*, *7*); and ~13.8 ka ago at Manis, Washington (*8*). However, the artifact assemblages from these ~14- to ~15-thousand-year-old North American sites are small and nondiagnostic, and lithic projectile points are absent. It was not until ~13 ka ago that the first recognizable and widespread North American archaeological traditions appeared, with people making lanceolate fluted points in central and eastern North America (Clovis Tradition) and others using stemmed projectile points in unglaciated western North America (Western Stemmed Tradition) (*9*, *10*). The connection between the artifact assemblages of the ~14- to ~15-thousand-year-old North American sites and later Clovis and Western Stemmed Traditions remains unclear. Here, we report a robust lithic projectile point assemblage from the layers dated between ~13.5 and 15.5 ka ago at the Debra L. Friedkin site, Texas (*11*), which has implications for the origin of both the ~13-thousand-year-old lanceolate and stemmed point traditions of North America.

RESULTS

Geology and geochronology

At the Debra L. Friedkin site, we excavated 104 m^2 of an area known as Block A, which is located on the second terrace flanking Buttermilk Creek (Fig. 1) (*11*). The Late Quaternary stratigraphy exposed by our excavations consists of colluvium resting on limestone bedrock, which in turn is buried by 1.2 to 1.4 m of unstratified clay that was deposited incrementally during overbank floods from Buttermilk Creek (Figs. 1 to 3). The archaeological record at the Friedkin site is buried in the upper portion of the floodplain clays, with up to 30 cm of archaeologically sterile sediments below the cultural horizons (Figs. 2 and 3).

The radiocarbon dating method was not used to date the archaeological components at the Friedkin site because there were no carbon samples that would yield reliable and accurate ages. In situ charcoal is not preserved, and all bones are leached of collagen. Dating of bulk sediment organics was not undertaken because these ages are usually inaccurate. For example, two bulk sediment ages from the Clovis horizon (unit 3a) at Excavation Area 8 of the Gault site, located ~400 m upstream of the Friedkin site, produced ages of 7130 ± 40 radiocarbon years before the present (^{14}C yr B.P.) (CAMS-65535; ~7.9 to ~8.0 ka ago) and 9300 ± 40 ^{14}C yr B.P. (CAMS-65986; ~10.4 to 10.6 ka ago) (*12*). These ages are 2 to 5 ka younger than the known age of Clovis.

Instead, the OSL dating method was used to determine the age of the artifacts at the Friedkin site by dating the floodplain sediments that bury them. This method is well suited for the site because according to the geological principle of inclusions, any items, such as artifacts, in an undisturbed sedimentary deposit, such as the floodplain clays at the Friedkin site, are at least as old as the sediments that contain them. The OSL method has been used for decades to date Late Quaternary deposits and has been shown to yield accurate ages;

[1]Center for the Study of the First Americans, Texas A&M University, College Station, TX 77843-4352, USA. [2]Department of Anthropology, Texas A&M University, College Station, TX 77843-4352, USA. [3]Department of Geosciences and Institute of Archaeology, Baylor University, Waco, TX 76798, USA. [4]Texas Archeological Research Laboratory, University of Texas, Austin, TX 78712, USA.
*Corresponding author. Email: mwaters@tamu.edu
†These authors contributed equally to this work.

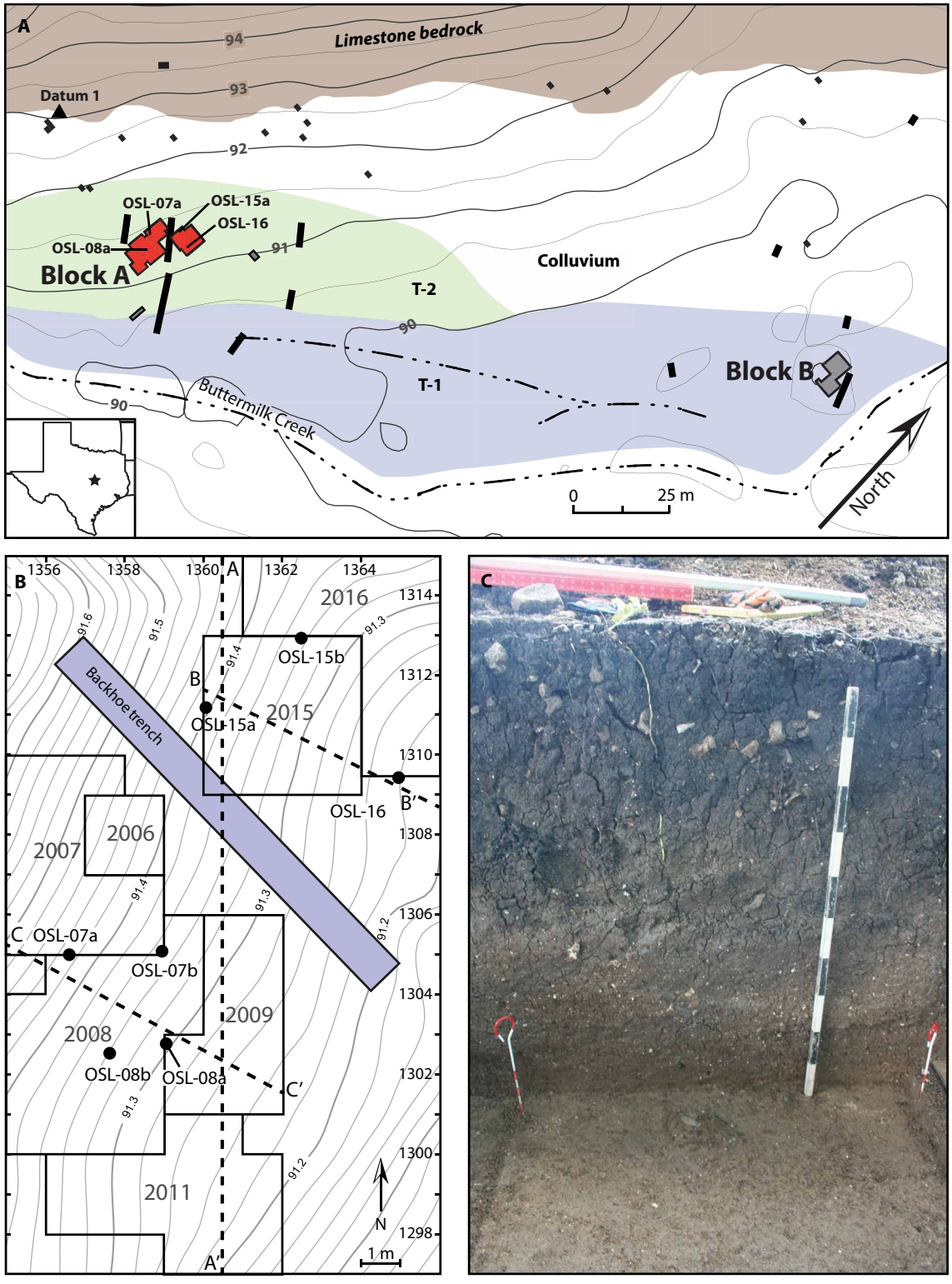

Fig. 1. Block A at the Debra L. Friedkin site. (**A**) Map showing the location of the Debra L. Friedkin site along Buttermilk Creek. The geomorphic setting of the site is shown along with the location of the excavated areas. The red-colored area is Block A. The location of the four optically stimulated luminescence (OSL)–dated columns is indicated. Solid squares and rectangles indicate the location of trenches and excavation units. T-1, Terrace 1; T-2, Terrace 2. The inset map shows the location of the Friedkin site in Texas. (**B**) Map of Block A excavation area and the year each area was excavated. OSL sample locations are shown. Geological sections A-A′, B-B′, and C-C′ are indicated with dashed lines and correlate with Figs.2 and 3. Modern topographic contours are shown with elevations in meters above datum (m AD). (**C**) Photograph of the floodplain sediments (north wall of excavation unit N1312 E1362). Late Archaic hearth feature occurs near the top of the section, and the complete lanceolate stemmed point (AM9875-2) dating ~15 ka ago is seen in the excavation unit at the base of the wall profile. Photo Credit: Michael Waters, Texas A&M University.

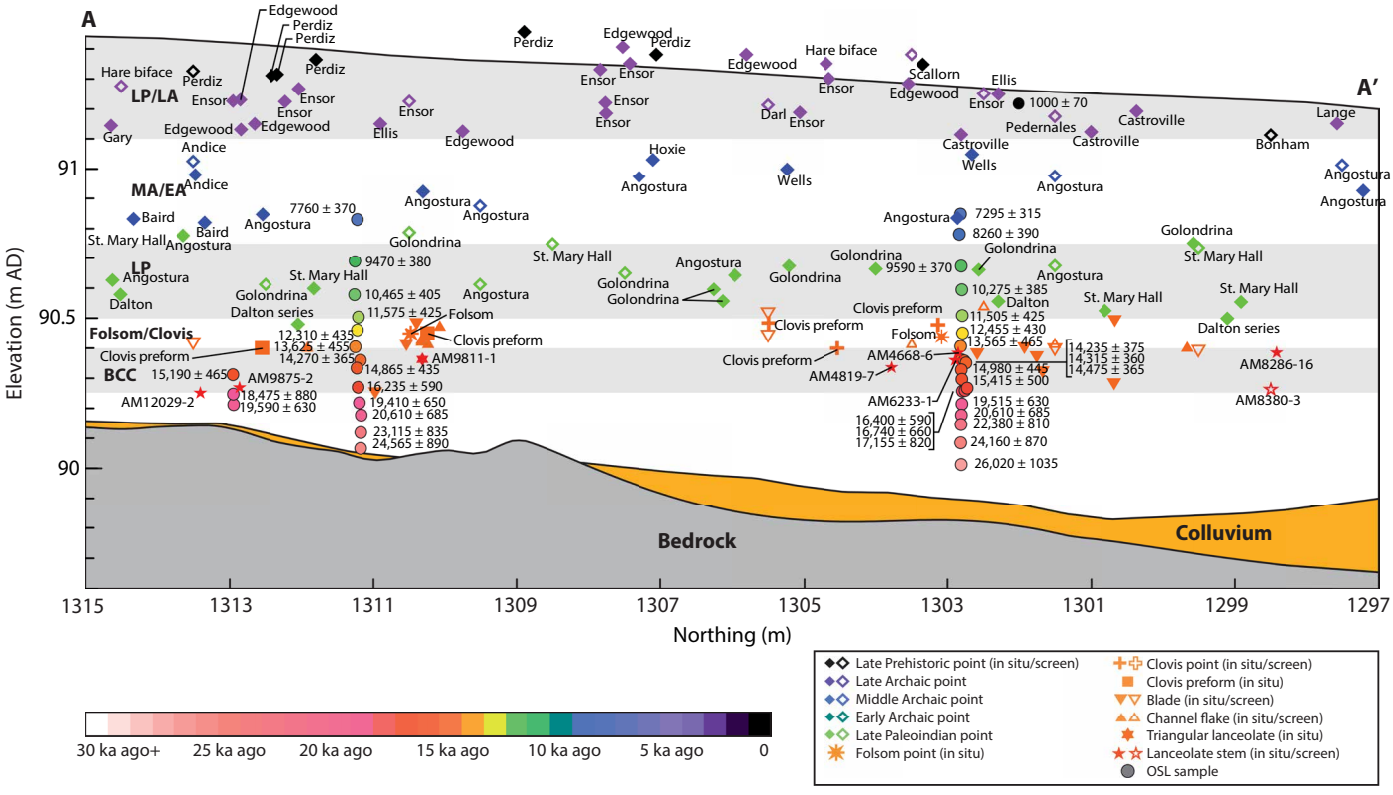

Fig. 2. Cross section A-A′ showing the site stratigraphy, location of time-diagnostic artifacts, and Bayesian-modeled OSL ages. Archaeological time periods are as follows: Late Prehistoric/Late Archaic (LP/LA), Middle Archaic/Early Archaic (MA/EA), Late Paleoindian (LP), Folsom/Clovis, and Buttermilk Creek Complex (BCC). Some Late Prehistoric and Late Archaic artifacts appear above the profile because there are places where the ground surface is higher than the contour line along the A-A′ profile (see Fig.1B for the location of this cross section). OSL ages from 2008 and 2015 are shown. The location of each pre-Clovis projectile point is identified, and the artifact number beginning with the designation AM allows identification of specific artifacts. This profile includes all artifacts 3.5 m west and east of the A-A′ line from 91.15 m AD to the surface because of the surface slope. All artifacts 5.5 m west and east of the A-A′ line between 90.5 and 91.5 m AD are shown because the deposits are horizontal. All artifacts 3.5 m west and east of the A-A′ line below 90.5 m AD are shown because the deposits slope to the east.

many tests have shown that OSL ages are in agreement with radiocarbon ages (*13*). Luminescence dating has also been used to successfully date archaeological sites in North America such as the Clovis horizon at Pavo Real, Texas, and the Archaic, Paleoindian, and pre-Clovis horizons at the Gault site, Texas (*12*, *14*, *15*).

The sediments at the Friedkin site are ideal for OSL dating because of the low-energy fluvial depositional environment. The slow incremental deposition on the floodplain and associated weak pedogenic alternation ensured solar resetting of sediment grains before burial. After burial, the sediments on the floodplain were minimally disturbed (*11*, *13*, *16*, *17*).

Seventy OSL ages were obtained from the Late Pleistocene and Early Holocene sediments of Block A (Figs. 1 to 3 and figs. S1 to S3). Thirty-eight OSL ages were previously published (*11*). Here, we present 32 new OSL ages obtained in 2015 and 2016 (table S1). Bayesian analyses of all OSL ages from four sediment columns yielded modeled ages with reduced SDs (fig. S1 and table S2). The Bayesian-modeled OSL ages are used to resolve a sediment deposition chronology and associated artifact ages (Figs. 2 and 3 and table S2). Correlation of Bayesian-modeled OSL ages and time-diagnostic artifacts shows that, in most areas of the site, floodplain sediments were horizontally deposited, but slope slightly upward at the northwest end of the 2007 excavation area and downward at the southeast end of the 2016 excavation area of Block A (Figs. 1 to 3).

Late Prehistoric to Clovis archaeological horizons

In this section, we discuss the post–13-thousand-year-old time-diagnostic artifacts and associated OSL ages from the floodplain sediments that overlie the deposits containing the pre-Clovis Buttermilk Creek Complex. This discussion provides an archaeological and chronological context for the pre-Clovis horizon and demonstrates the archaeological integrity of the deposits at the Debra L. Friedkin site and the accuracy of the OSL ages.

In the upper 0.8 to 1.1 m of the floodplain sequence at Block A, we recovered over 639,000 artifacts, including over 4600 tools, of which 130 are time diagnostic (mostly projectile points). The position of the time-diagnostic artifacts is collapsed onto three transects across different portions of Block A (Figs. 2 and 3). These artifacts group into four mutually exclusive zones that correspond to the prehistoric cultural periods of central Texas (*18*, *19*). These zones occur in chronological order, with Late Prehistoric and Late Archaic artifacts occurring near the surface, followed by a zone with only Middle Archaic and Early Archaic artifacts, then by a deeper zone with Late Paleoindian point types, and below this a zone containing only Folsom and Clovis artifacts (Figs. 2 and 3). In situ diagnostics of one zone are not found in overlying or underlying zones. Within a zone, most projectile points are in correct chronological order. This shows that there were sequential occupations on the Buttermilk Creek floodplain that were incrementally buried over time by sediment during repeated overbank

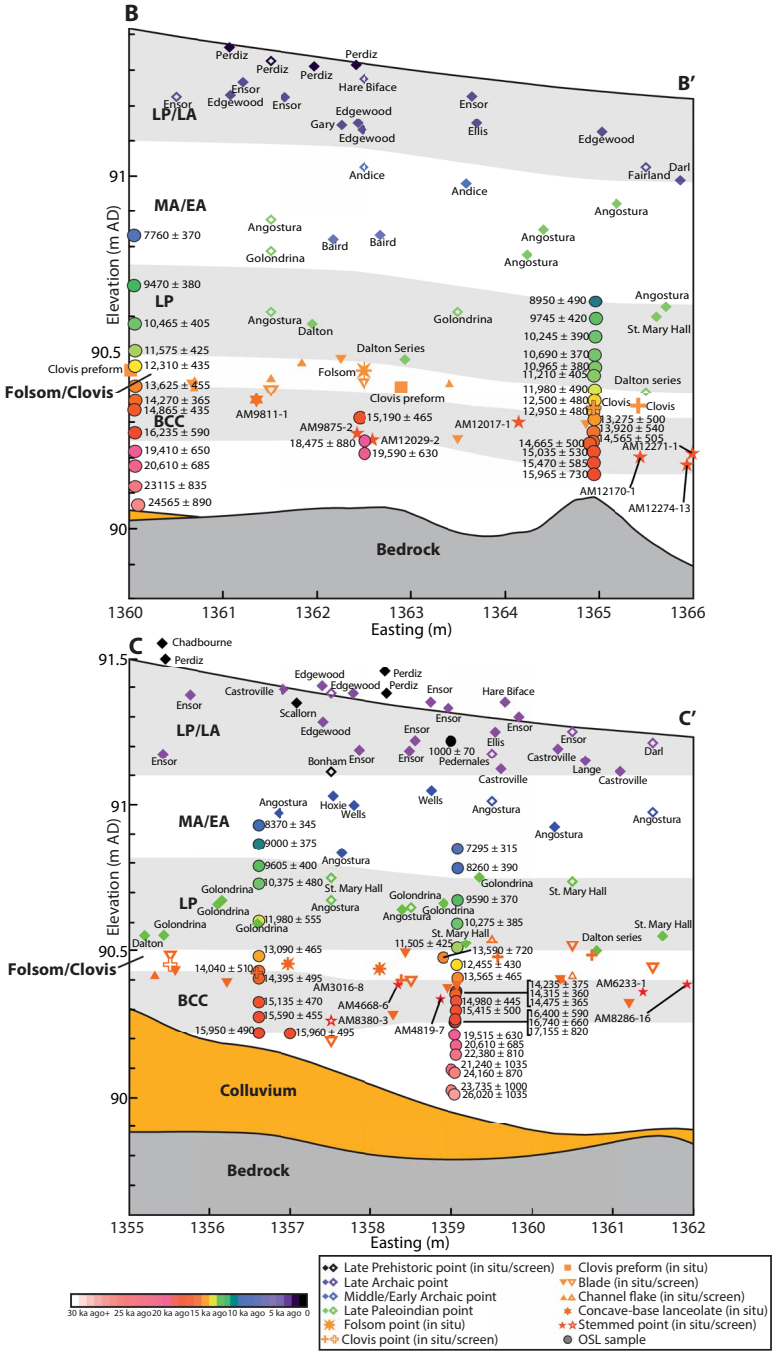

Fig. 3. Cross sections B-B′ and C-C′ showing the site stratigraphy, location of time-diagnostic artifacts, and Bayesian-modeled OSL ages. Archaeological time periods are as follows: Late Prehistoric/Late Archaic (LP/LA), Middle Archaic/Early Archaic (MA/EA), Late Paleoindian (LP), Folsom/Clovis, and Buttermilk Creek Complex (BCC). Some Late Prehistoric and Late Archaic artifacts appear above the C-C′ profile because there are places where the ground surface is higher than the contour line along this transect (see Fig. 1B for the location of these cross sections). The location of each pre-Clovis projectile point is identified, and the artifact number beginning with the designation AM allows identification of specific artifacts. The B-B′ profile includes all OSL ages and artifacts from the areas excavated in 2015 and 2016. The C-C′ profile includes all OSL ages and artifacts from the areas excavated in 2007, 2008, 2009, and 2011.

events over the last 13 ka. Since burial, these zones have remained intact with minimal disturbance.

In central Texas, the Late Prehistoric period postdates ~0.65 ka ago, and the Late Archaic period dates between ~0.65 and ~4.2 ka ago (*18*, *19*). Diagnostic artifacts associated with these two cultural periods are used as the basis for identifying a Late Prehistoric/Late Archaic zone in the uppermost portion of the site (Figs. 2 to 4). The Late Prehistoric period is recognized by 10 time-diagnostic projectile points: 7 Perdiz, 1 Scallorn, 1 Bonham, and 1 Chadbourne. The Late Archaic is represented by 35 time-diagnostic projectile points: 2 Darl, 7 Edgewood, 2 Ellis, 14 Ensor, 1 Fairland, 1 Gary, 4 Castroville, 1 Lange, 1 Pedernales, and 2 Hare bifaces. The age range of only a

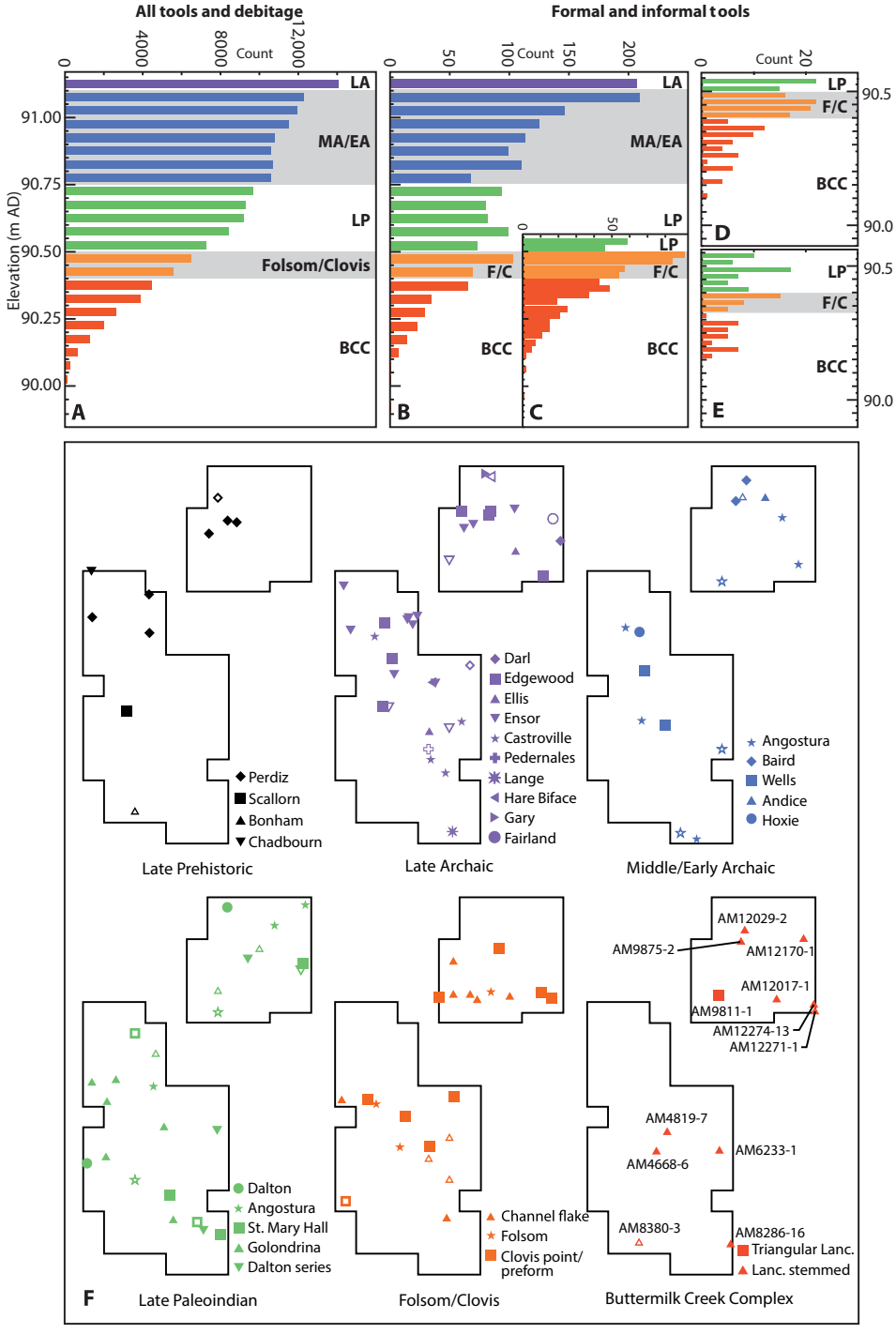

Fig. 4. Lithic artifact counts by depth and maps of diagnostic artifacts for Block A. (**A**) Total artifacts from 52 units with comparable data for all horizons excavated between 2009 and 2016, including all tools and debitage >0.625 cm in size, by 5-cm levels for the Late Archaic (LA), Middle/Early Archaic (MA/EA), Late Paleoindian (LP), Folsom/Clovis (F/C), and Buttermilk Creek Complex (BCC) horizons. (**B**) Total formal and informal tools from 52 units with comparable data for all horizons excavated from 2009 to 2016 (>0.625 cm in size) by 5-cm levels. (**C**) Counts of formal and informal tools from all 104 units from 2006 to 2016 (>0.625 cm in size for only the LP, F/C, and BCC layers) at 2.5-cm levels. Occurrence of artifacts below 90.15 m AD is accounted for by the slope of the BCC artifact–bearing deposits. (**D**) Counts of formal and informal tools from 2015 to 2016 excavations >0.625 cm in size for the LP, F/C, and BCC layers west of E1363. (**E**) Counts of formal and informal tools from 2015 to 2016 excavations >0.625 cm in size for the LP, F/C, and BCC layers east of E1363. (**F**) Horizontal distribution of diagnostic artifacts by archaeological component for Block A.

few of these types is known: Darl, ~0.65 to ~1.3 ka ago; Ensor and Edgewood, ~1.3 to ~2.1 ka ago; Castroville, ~2.1 to ~3.1 ka ago; and Pedernales, ~3.1 to ~4.2 ka ago (*19*). A single OSL age of 1000 ± 70 yr B.P. (UIC2352; Figs. 2 and 3 and table S2) was obtained from the Late Prehistoric and Late Archaic horizon associated with the Ensor and Ellis points at the Friedkin site. This age is in general agreement with the known age for these types. Forty-four Late Prehistoric and Late Archaic points are in chronological order (Figs. 2 and 3). Four points (one Pedernales, one Bonham, one Darl, and one Castroville) are out of chronological order within the Late Prehistoric and Late Archaic zone. This type of mixing of Late Prehistoric and Late Archaic point types in central Texas sites is common because of repeated use of cooking features during the Late Holocene [e.g., (*18*, *20*)]. In the Late Prehistoric and Late Archaic zone at the Friedkin site, there are a number of burned rock features with fire-cracked rock (as seen in Fig. 1C). The reuse of these features likely accounts for mixing of the few points within this zone.

In central Texas, the Middle Archaic dates between ~4.2 and ~5.7 ka ago, and the Early Archaic dates from ~5.7 to ~8.6 ka ago (*18*–*20*). In the Middle Archaic and Early Archaic zone at the Friedkin site, 15 time-diagnostic Early Archaic projectile points were recovered (Figs. 2 to 4). This horizon includes two Andice, two Wells, one Hoxie, two Baird (Early Triangular), and eight Angostura points. Most Early Archaic point types are poorly dated in Texas, but Andice is well dated to ~5.7 to ~6.0 ka ago (*19*). Baird (Early Triangular) points are tentatively dated to the beginning of the Middle Archaic ~5.5 to ~5.6 ka ago (*19*), but this type was recently dated at Hall's Cave, Texas, to ~8.6 ka ago (*21*), showing that it spans both the Middle Archaic and Early Archaic. Angostura is poorly dated but is generally thought to be a long-used type spanning the Early Archaic to the Late Paleoindian periods from ~8.6 to ~10.4 ka ago (*18*, *22*, *23*). At the Friedkin site, these point styles are generally in chronostratigraphic order, with two Andice points occurring with two Wells points near the top of this zone, two Baird points below these, and eight Angostura points in the lowest portion of the Middle Archaic and Early Archaic zone.

Six OSL ages from the Middle Archaic and Early Archaic horizon at the Friedkin site range from 7295 ± 315 yr B.P. (UIC2360) to 9000 ± 375 yr B.P. (UIC2061; Figs. 2 and 3 and table S2). An age of 7760 ± 370 yr B.P. (BG4066) occurs in close proximity to the Baird points, and this date falls within the age range for this type (Figs. 2 and 3). Angostura points are associated with all six OSL ages; four ages overlap with the known minimum age for Angostura (~8.6 ka ago), but two OSL ages appear too young for Angostura. This suggests that either this type extends later in time or some of the Angostura points at the Friedkin site may be intrusive into the youngest Early Archaic sediments. It is not uncommon for older projectile point types to be found in a younger cultural context because prehistoric people would sometimes pick up older points from the surface and bring them to their camps. This also holds true for the Golondrina point found at the base of this layer in close proximity to the Late Paleoindian boundary.

Below the Middle Archaic and Early Archaic zone is a 25-cm-thick zone with Late Paleoindian diagnostic artifacts, known to date ~9 to 12 ka ago in central Texas (*18*, *20*, *22*, *23*). The Late Paleoindian zone at the Friedkin site contains five Angostura, five St. Mary Hall, nine Golondrina, and five Dalton/Dalton series points (Figs. 2 and 4). Angostura, St. Mary Hall, and Golondrina points co-occur in the upper and middle portions of the Late Paleoindian zone. These types are poorly dated, but estimates place Golondrina at ~9.6 to ~11.2 ka ago, St. Mary Hall at ~9.8 to ~11.5 ka ago, and Angostura at ~8.6 to 10.4 ka ago (*18*, *22*, *23*). These types commonly co-occur at sites such as the Wilson-Leonard site, located 40 km from the Friedkin site, where Golondrina, St. Mary Hall, and Angostura types overlap in deposits radiocarbon dated between ~9.7 and ~11.1 ka ago (*20*). Near and at the base of the Late Paleoindian zone at the Friedkin site are Dalton/Dalton series points that are radiocarbon dated elsewhere to between ~11.2 and ~12 ka ago (*18*, *22*, *23*). Fourteen OSL ages, ranging from 9590 ± 370 yr B.P. (UIC2363) to 11,980 ± 555 yr B.P. (UIC2048; Figs. 2 and 3 and table S2), are from the Late Paleoindian horizon at the Friedkin site. These OSL dates encompass the known ages for the various Late Paleoindian projectile point types. More specifically, 10 OSL ages ranging from 9590 ± 370 yr B.P. (UIC2363) to 10,965 ± 380 yr B.P. (BG4207; Figs. 2 and 3 and table S2) are associated with the Angostura, St. Mary Hall, and Golondrina types and overlap well with the radiocarbon ages from Wilson-Leonard and other sites where these types co-occur. The OSL ages ranging from 11,210 ± 405 yr B.P. (BG4206) to 11,980 ± 555 yr B.P. (UIC2048) occur in the zone with the Dalton/Dalton series points (Figs. 2 and 3) and again agree well with the known age for Dalton at other sites. One Dalton point was found in the middle of this zone and appears out of context. Again, it is not uncommon to find old time-diagnostic projectile points in younger contexts at sites in central Texas [e.g., (*20*)].

A 10-cm-thick zone with Folsom and Clovis artifacts occurs below the Late Paleoindian horizon (Figs. 2 and 3). Near the top of this zone are a Folsom point fragment and two late-stage Folsom preform flute failures (fig. S4). These Folsom artifacts are separated up to 9 m horizontally (Fig. 4F) but only 1.7 cm vertically. Underlying these Folsom lithics are time-diagnostic Clovis artifacts that include the following: (i) 1 end thinned, concave base, projectile point base (AM12018-1); (ii) 1 point midsection with channel flake scar terminations on each face (AM4447-1); (iii) 5 point fragments; (iv) 17 preforms and secondary bifaces with overshot and overface flaking, with some showing squared and beveled bases, and end thinning scars; and (v) 10 blades and blade segments (figs. S4 and S5). In addition, nine channel flakes were recovered. Seven were found within the Folsom and Clovis zone, one was found <2.5 cm below the lower boundary, and one was found <5 cm above the upper contact of this zone (Figs. 2 and 3). The Clovis point base (AM12018-1) is within 20 cm of the 2016 column of OSL ages and is bracketed by ages of 12,500 ± 480 yr B.P. (BG4209) and 12,950 ± 480 yr B.P. (BG4218). Seven ages from the Folsom-Clovis zone range from 11,980 ± 490 yr B.P. (BG4208) to 13,590 ± 720 yr B.P. (UIC2059; Figs. 2 and 3 and table S2). These ages fall within the known age range for Folsom (~12.2 to 12.7 ka ago) and Clovis (~12.7 to ~13 ka ago) (*7*). Overall, these results show that within the Late Prehistoric to Clovis horizons at the Friedkin site, the relative order of time-diagnostic artifacts matches the known cultural chronology for central Texas, and the known ages for time-diagnostic artifacts overlap with OSL ages.

Buttermilk Creek Complex horizon

About 100,000 artifacts, including 328 tools and 12 complete and fragmentary projectile points of the Buttermilk Creek Complex, were excavated from the floodplain clays, 15 to 20 cm below the Folsom-Clovis zone (Figs. 2 to 5). These artifacts are dated to ~13.5 and ~15.5 ka ago by 19 OSL ages (table S2). The deepest floodplain clays are OSL dated to >16 ka ago (n = 13) and have no in situ artifacts (Figs. 2 and 3 and table S2) (*11*). The artifacts comprising the Buttermilk

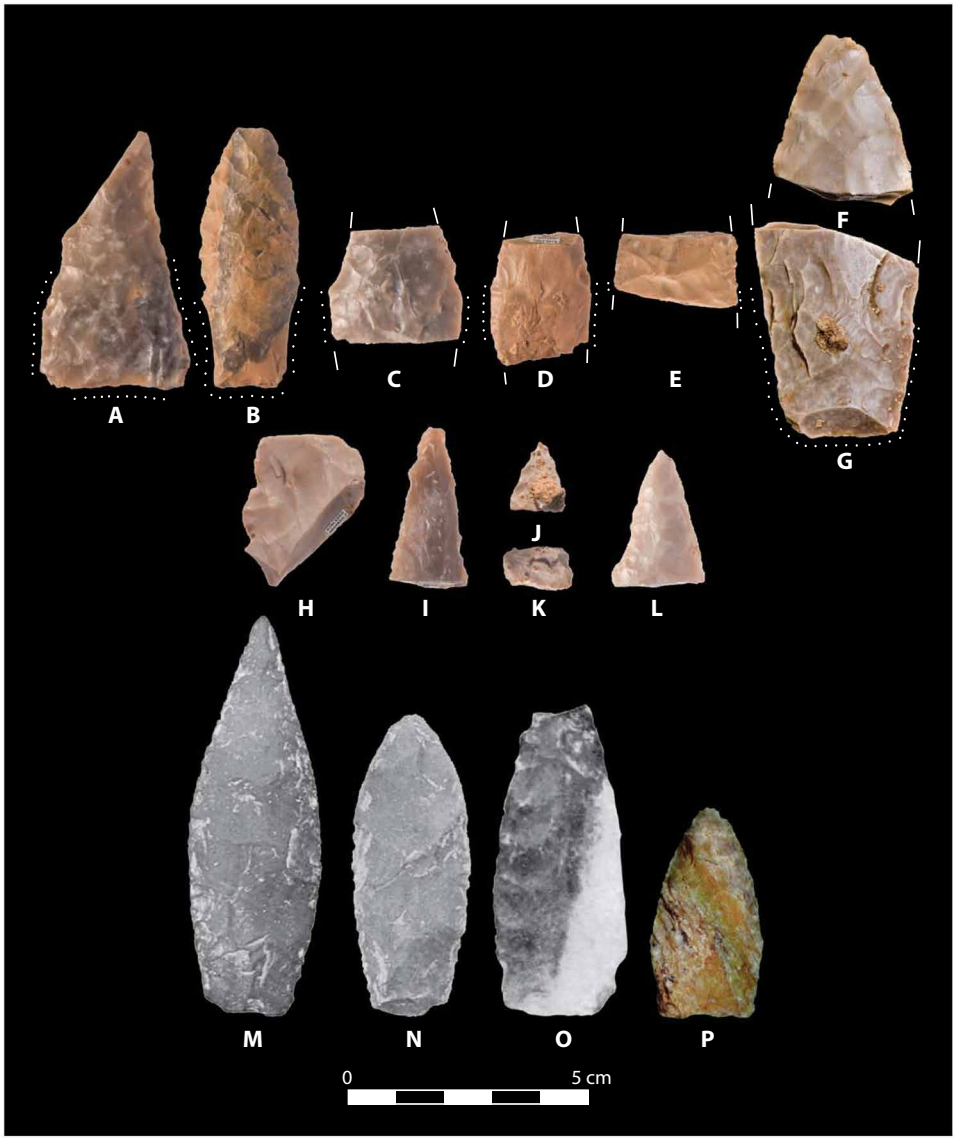

Fig. 5. Pre-Clovis projectile points from the Debra L. Friedkin site and other sites in North America. (**A**) Triangular lanceolate point (AM9811-1), (**B**) lanceolate stemmed point (AM9875-2), (**C**) lanceolate stemmed point midsection with base and blade sections (AM12017-1), (**D**) lanceolate stemmed point midsection with base and blade sections (AM6233-1), (**E**) lanceolate stemmed point midsection with base and blade sections (AM12271-1), (**F**) point tip (AM4668-6), (**G**) lanceolate stemmed point base (AM8286-16), (**H**) point midsection (AM4819-7), (**I**) beveled point tip (AM12170-1), (**J**) beveled point tip (AM8380-3), (**K**) beveled point tip midsection (AM12029-2), and (**L**) point tip (AM12274-13). (**M**) Point from Iztapan Mammoth II, Mexico [from (*29*)], (**N**) point from Iztapan Mammoth II, Mexico [from (*29*)], (**O**) point from Iztapan Mammoth I, Mexico [from (*29*)], and (**P**) Miller point from Meadowcroft Rockshelter, Pennsylvania.

Creek Complex assemblage are described elsewhere (*11*, *24*). Here, we describe the Buttermilk Creek Complex projectile point assemblage that includes lanceolate stemmed and triangular lanceolate forms (Fig. 5 and fig. S6). We also discuss the associated Buttermilk Creek Complex bifaces (fig. S7).

Lanceolate stemmed points include one complete specimen, one base fragment, four medial fragments, and five tips (Fig. 5, fig. S6, and table S3). The complete point (AM9875-2) was resharpened but appears to reflect its original size and morphology. The blade of the point is alternately beveled with convex lateral edges. The hafting element is stemmed with ground concave lateral edges and a ground concave base that was thinned by removing multiple short flakes from each face. The base fragment (AM8286-16) has a contracting stem with a subtle concave base. The edges and base of the stem are ground. A subtle shoulder is present where the blade expands outward from the base. The four medial fragments (AM12017-1, AM6233-1, AM12271-1, and AM4819-7) repeat the characteristics of the complete specimen with a beveled blade and a ground and contracting stem. These fragments show that as resharpening occurred, the blades became beveled and indented relative to the base. Four point tips (AM12029-2, AM8380-3, AM4668-6, and AM12170-1) are alternately beveled and are consistent with the morphology of the blades displayed by the complete point and three medial fragments. Distal fragment AM12274-13 is not beveled. All specimens show microscopic

use-wear consistent with hafting and use as projectile points (fig. S8). It is important to note that lanceolate stemmed points are confined exclusively to the Buttermilk Creek Complex horizon; none are found in the post–13-thousand-year-old sediments. The lanceolate stemmed points of the Buttermilk Creek Complex closely resemble an undated Texas projectile point type defined as "Early Stemmed Lanceolate" (*25*).

Lanceolate stemmed points at the Friedkin site are confined to the clays dating between ~13.5 and ~15.5 ka ago (Figs. 2 and 3 and table S2). Seven of the 11 projectile points and point fragments occur in close proximity to specific OSL ages. Three OSL ages temporally bracket the complete point (AM9875-2) that rested horizontally on older floodplain clays; the two ages below the point are 18,480 ± 880 yr B.P. (BG3994) and 19,410 ± 650 yr B.P. (BG4076), and, at 3 cm above this point, the age is 15,190 ± 465 yr B.P. (BG3995). Likewise, a beveled point tip midsection (AM12029-2) was bracketed by these same three ages. One medial point fragment (AM12271-1) lies 50 cm horizontally from the age of 15,035 ± 530 yr B.P. (BG4263), one point tip (AM12274-13) lies 50 cm away from the age of 15,470 ± 590 yr B.P. (BG4238), and one medial fragment (AM12017-1) lies between ages 13,280 ± 500 yr B.P. (BG4219) and 13,920 ± 540 yr B.P. (BG4220). Another point tip (AM4668-6) lies 65 cm west of the 2008 column of OSL ages and between sediments dated to 13,565 ± 465 yr B.P. (UIC2354) and 14,235 ± 375 yr B.P. (UIC2367) and at the same elevation as sediments dated to 13,565 ± 465 yr B.P. (UIC2354). A point midsection (AM4819-7) lies 1 m north of the 2008 column of OSL ages, is bracketed between ages 14,315 ± 360 yr B.P. (UIC2369) and 14,980 ± 445 yr B.P. (UIC2359), and is at the same elevation and in the same sediments that yielded an age of 14,475 ± 365 yr B.P. (UIC2350). The other point fragments (AM12170-1, AM6233-1, AM8380-3, and AM8286-16) occur 2.4 to 5.3 m from the nearest OSL column. These points lie in the horizon dated between ~13.5 and ~15.5 ka ago.

A broken triangular lanceolate projectile point (AM9811-1) occurs in the uppermost portion of the clays ranging in age from ~13.5 to ~14 ka ago, below the Clovis horizon (Fig. 5A, fig. S6, and table S3). This point lacks the distal tip due to a diagonal snap fracture that probably resulted from impact. The remaining lateral blade edges are gently concave with a pronounced alternate bevel. The haft element has straight lateral edges that expand outward with a concave base. The haft edges and base are ground. The base is thinned on both sides by irregular, flute-like flakes that extend upward. This point was heavily used and resharpened; use-wear analysis shows that it was hafted and used as a projectile (fig. S8). This point was found at the same elevation and 1 m south of the OSL age 14,270 ± 365 yr B.P. (BG4017). A second age 13,625 ± 455 yr B.P. (BG4019) was obtained 4.5 cm above the point.

Forty late-stage biface fragments were found in the ~13.5- to ~15.5-thousand-year-old sediments. Of these, 13 are large enough to provide insights into the production of stemmed lanceolate points (fig. S7 and table S3). Most flake scars on these bifaces terminate at the midline, but five bifaces show flakes crossing over the midline of the biface (overface flaking) and two display a rolled edge from an overshot flake removal. Two overshot flakes were found in the same deposits. The bifaces show no evidence of end thinning or preparation of a beveled base for later fluting. All bifaces are plano-convex in cross section, indicating that lanceolate stemmed points were made from flake blanks that were bifacially reduced by lateral thinning. Similarities and differences exist between the pre–13-thousand-year-old and Clovis bifaces at the Friedkin site. Both exhibit overface and overshot flaking, reflecting similar biface thinning strategies; however, these flaking techniques were used with greater frequency to produce Clovis preforms. End thinning and base beveling in preparation for end thinning found on Clovis preforms are absent in the pre–13-thousand-year-old biface assemblage. The pre–13-thousand-year-old bifaces are predominately made on large flake blanks, whereas the Clovis bifaces were made from both nodules and flake blanks.

In addition to the points and other bifaces, the ~13.5- to ~15.5-thousand-year-old assemblage at the Friedkin site also includes blade segments, bladelets, scrapers, bifacial discoidal cores, and snap fracture tools (radial and bend break) most commonly made on flakes but also bifaces, retouched flakes, expedient tools, and ground hematite. This assemblage, combined with the newly described projectile points, makes up the Buttermilk Creek Complex (*11*, *24*). This assemblage compares well with the pre-Clovis assemblage from the Gault site (*15*).

Integrity of the Late Prehistoric to Buttermilk Creek Complex horizons

Previous studies of the geology, pedology, micromorphology, and magnetic properties of the site's sediments show that the deposits at the Friedkin site are minimally disturbed by postdepositional processes (*11*, *16*, *17*). Despite this evidence, the stratigraphic integrity of the deposits has been questioned, and it has been suggested that artifacts moved downward through the profile, resulting in the mixing of the artifacts at the site and creating the layer that is identified as the Buttermilk Creek Complex horizon (*26*). The superposition of cultural time horizons described for the Late Prehistoric through Clovis horizons at the site based on the distribution of 130 time-diagnostic artifacts shows that downward movement of large artifacts, such as projectile points, did not occur. If downward movement had taken place over time, then we should expect to see multiple time-diagnostic artifacts from the overlying horizon within the cultural zone immediately beneath it and associated with older ages, but this is not the case. Furthermore, a previous study of artifact size classes with depth at the Friedkin site (*11*, *16*) showed no change in relative size class from the surface down to 90.225 m AD for artifacts larger than 0.625 cm in diameter. In short, 130 time-diagnostic artifacts within the Late Prehistoric to Clovis horizons, coupled with all other previous studies (*11*, *16*, *17*), show that downward movement of artifacts did not take place at the site. In addition, the OSL ages associated with each cultural zone agree with the known age of the time-diagnostic artifacts found in each zone, demonstrating the accuracy of these ages.

Variation in the number of formal tools with depth also demonstrates the presence of intact cultural horizons at the Friedkin site. A site with intact occupation surfaces usually has fluctuating quantities of tools with depth representing either successive periods of occupation and abandonment or shifting site usage over time. A site with substantial mixing of younger artifacts from a single occupation into older contexts, such as Clovis artifacts moving downward to create the Buttermilk Creek Complex horizon, should show a single mode with a decline in artifact numbers and a general decrease in the size of artifacts with depth (*27*).

At the Friedkin site, there is a general increase through time in total lithic tools and debitage that appears to reflect a continuous increase in lithic reduction activity from the Late Pleistocene through the Holocene because of either increasing human populations or increasing site occupation span and decreasing mobility over time (Fig. 4A). This pattern is often seen at other North American sites with multiple occupation episodes [e.g., *20*)]. Intense use of the Friedkin site over time combined with slow deposition has resulted in no clear

indication of multimodal distribution of artifacts when all tools and debitage are considered (Fig. 4A). When only the quantities of formal and informal tools with depth are plotted (Fig. 4, B and C), multiple modes of artifact concentrations appear, which suggest changes in local lithic reduction activities through time. A large increase in tools at 90.50 to 90.45 m AD correlates with the top of the Folsom and Clovis horizon—with two smaller peaks below this, at 90.375 to 90.35 m AD and 90.30 to 90.275 m AD, that seem to reflect separate occupation episodes in the Buttermilk Creek Complex horizon. In the 2015–2016 excavation area where the sediments slope, we divided this assemblage into two samples along the E1363 line. When the number of formal and informal tools is plotted with depth, the same peaks in the number of tools are still present but offset ~10 cm due to slope (Fig. 4, D and E). These distributions again show that artifacts have remained in their original context, albeit on a sloping surface in the 2015–2016 block excavation. These lines of evidence demonstrate that there has been minimal to no movement of artifacts between cultural zones at the site, that the OSL ages from the site are accurate, and that there is an in situ cultural horizon predating Clovis at the site.

DISCUSSION

In 1949, excavations at Blackwater Draw showed that Clovis projectile points occurred in a layer stratigraphically below one containing Folsom points. It was not until many years later that Clovis was dated to ~12.7 to ~13 ka ago and Folsom ~12.2 to ~12.7 ka ago (*7*). Here, we reported an assemblage of stemmed projectile points associated with other artifacts, below a Folsom and Clovis artifact–bearing layer at the Debra L. Friedkin site along Buttermilk Creek, Texas, dated to ~13.5 to ~15.5 ka ago. Also, along Buttermilk Creek, in similar deposits just 250 m upstream of Block A at the Friedkin site, stemmed projectile points dated to ~16 ka ago are reported below a Clovis horizon at Area 15 of the Gault site, Texas (*15*). The earliest stemmed points elsewhere in North America occur in the Intermountain West at Paisley Caves, Oregon (Fig. 6A). These Western Stemmed

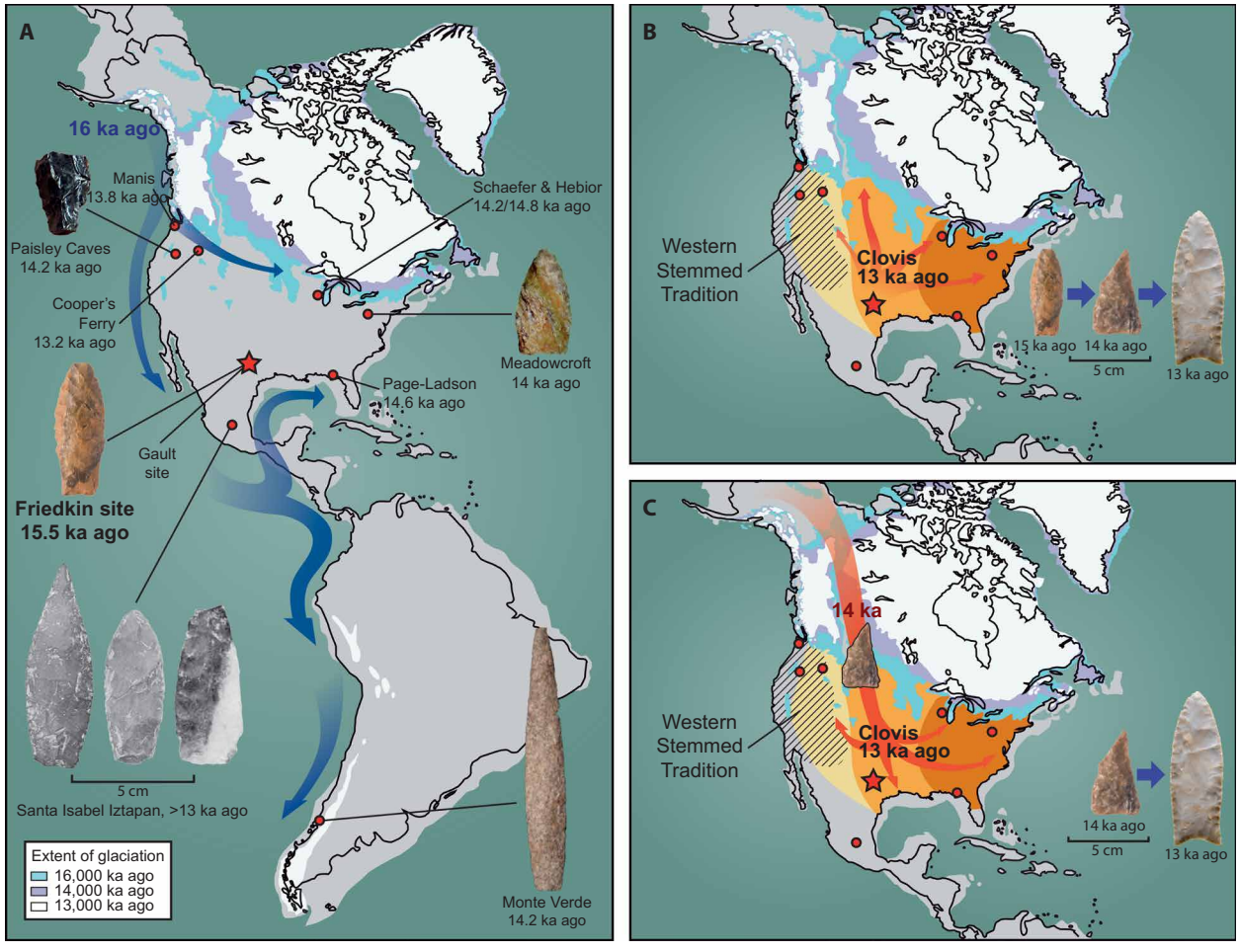

Fig. 6. Proposed models explaining the peopling of the Americas. (**A**) The earliest people exploring the Americas used stemmed projectile points and traveled along the coast ~16 ka ago, moved inland, and reached the Debra L. Friedkin site by ~15.5 ka ago and South America by ~14.2 ka ago (blue arrows). (**B**) A triangular lanceolate projectile point form develops in situ from the earlier lanceolate stemmed form ~14 ka ago, with Clovis developing ~13 ka ago and spreading across most of the United States and northern Mexico (red arrows). (**C**) Alternatively, the origin of Clovis may be explained by a second migration that occurs with people using triangular lanceolate points traveling through the ice-free corridor and reaching the Friedkin site by ~14 ka ago. Clovis develops in situ ~13 ka ago and spreads across central and eastern North America (red arrows). Archaeological sites with ages are shown. Colored regions on the map show the general distribution of Clovis, with highest densities in the east (brown), moderate densities in the central United States (orange), and light densities in the west (yellow), overlapping with the Western Stemmed Tradition shown by the cross-hatch pattern.

Tradition projectile points are at least contemporaneous with Clovis, dated to ~12.7 to ~13 ka ago (*9*). The oldest occupation at Paisley Caves includes artifacts and human coprolites that date to ~14.2 ka ago. No projectile points were found in the earliest layers of the site, but the only diagnostic lithic technology present at Paisley Caves is related to the Western Stemmed Tradition. This, combined with the lack of diagnostic Clovis technology in the site assemblage, suggests that stemmed points may date to the earliest occupation at Paisley Caves (*9*). At Cooper's Ferry, Idaho, stemmed points are reported to date to ~13.2 ka ago (Fig. 6) (*28*), but additional chronological information is needed to confirm this proposed age. At Meadowcroft Rockshelter, Pennsylvania (Fig. 6A), the Miller point (Fig. 5P) with its subtle shoulder and short stem may be dated to ~14 ka ago (*7*), but this age remains to be confirmed. In Mexico, a stemmed projectile point (Fig. 5O), along with other artifacts, was associated with the bones of a single mammoth buried in undisturbed lacustrine sediments at Santa Isabel Iztapan I (Fig. 6A) (*29*, *30*). Four hundred meters away, at Santa Isabel Iztapan II, two stemmed points (Fig. 5, M and N) were associated with butchered mammoth bones in the same lacustrine sediments (*29*). The Iztapan sites are not directly dated, but dated tephra layers bracketing the mammoth remains and associated artifacts suggest that they fall between ~14.5 and ~10.8 ka ago (*30*). In South America, there is a long history of the use of stemmed points by the earliest inhabitants of the continent and their descendants. At Monte Verde, Chile (Fig. 6A), people used stemmed El Jobo projectile points by ~14.2 ka ago (*7*), with El Jobo and later stemmed Fishtail points becoming widespread across South America ~13 ka ago (*31*).

The evidence from Friedkin, Gault, and other sites suggests that the earliest known people to enter the Americas were using stemmed points. These people likely arrived by traversing the Pacific coast using watercraft (Fig. 6A) (*10*, *32*). This corridor would have been open for migration by ~16 ka ago as the Cordilleran Ice Sheet retreated and exposed tracks of land along the coast (*32*). The interior corridor between the Cordilleran and Laurentide ice sheets did not open until ~14 ka ago, and bison and other animals were passing through the corridor by ~13 ka ago (*32*). The ice-free corridor did not open soon enough to explain the presence of people south of the ice before ~14 ka ago.

As people occupied the coast, some began to move inland (Fig. 6A). By ~13.8 ka ago, they were on the Olympic Peninsula of Washington as witnessed by the Manis site. Traveling close to the ice margin, people are present in Wisconsin by ~14.8 and ~14.2 ka ago and in Pennsylvania by ~14 ka ago. By ~14.2 ka ago, people trekked into the northern Great Basin, as witnessed by Paisley Caves. Farther south, people made their way to the Valley of Mexico, as witnessed by the Iztapan Mammoth sites. Some people appear to have entered the Gulf of Mexico and made their way to Page-Ladson by ~14.6 ka ago. Others moved inland and discovered the Friedkin and Gault sites by ~15.5 ka ago. Some groups, carrying stemmed El Jobo points, continued south and reached the southern portion of South America by ~14.2 ka ago.

A new point form, a triangular lanceolate point, appears at the Friedkin site by ~14 ka ago. This form could have developed in situ from the earlier lanceolate stemmed point and could be the precursor to the lanceolate, fluted Clovis point. Similarities exist between the bifaces and tool assemblages of the Buttermilk Creek Complex and Clovis and may suggest that Clovis emerged in situ from the Buttermilk Creek Complex (*11*, *24*). Once developed, lanceolate fluted concave base point technology could have rapidly spread over the eastern two-thirds of North America and into northern Mexico, while people using stemmed points remained in the western third of the continent where that technology developed into the distinct Western Stemmed Tradition by ~14 ka ago (Fig. 6B). During this time, people continued to use stemmed points in South America.

Alternatively, the stemmed and lanceolate point traditions of North America may represent two separate human migrations that took different routes south of the continental ice sheets and accessed and settled different parts of the unglaciated continent at the end of the Pleistocene (Fig. 6C) (*33*). Stemmed points could have arrived with the first people to settle the Pacific and Gulf coasts, while other groups carrying some form of lanceolate point could have entered later through the inland, ice-free corridor (*33*). The progenitor of the ~13-thousand-year-old Clovis concave base, fluted, lanceolate point may have been a triangular lanceolate point such as the one found at the Friedkin site. The age associated with this point form at the Friedkin site may indicate the arrival of lanceolate points ~14 ka ago, with later in situ development of Clovis from this point form by ~13 ka ago.

Both models are compatible with the current human genetic evidence and what is known about the opening of the coastal and inland corridors (*1*, *2*, *32*). More excavations of buried and datable Late Pleistocene sites are needed to find the archaeological data and materials for genetic testing that will test our hypotheses and continue to decipher the complex story of the first Americans.

MATERIALS AND METHODS

Excavation and curation

Excavations at the area known as Block A took place in 2006, 2007, 2008, 2009, 2015, and 2016. During this time, 104 m^2 of this area was excavated (Fig. 1B). Standard archaeological excavation methods were used at the Debra L. Friedkin site, Texas (41BL1239). Excavation units were 1 m by 1 m and were designated by their southwestern corner coordinates that were determined from an arbitrary datum originally established at the Gault site. Generally, the upper portions of the units were excavated in 5- and 2.5-cm levels in the Paleoindian levels. Artifacts larger than ~1.5 cm were generally mapped in place in the Paleoindian levels, and the elevation was determined relative to the site datum. In the Late Prehistoric and Archaic levels, diagnostic artifacts and features were mapped. The sediment excavated from each level was screened through one-quarter inch (6.35 mm) mesh, and a sample from the southwest corner was additionally screened through one-eighth inch (3.175 mm) mesh. All artifacts were assigned a unique catalog number (the letters "AM," followed by a number) that ties the artifact to a specific unit and level. All artifacts were washed, processed, and cataloged in the Center for the Study of the First Americans laboratories. All artifacts were curated in the Center for the Study of the First Americans at Texas A&M University.

OSL dating

Sediments targeted for OSL dating are clay-rich distal overbank sediments in close association with artifact-bearing levels. Because these sediments did not contain a sand (2000 to 63 μm) fraction or appreciable coarse silt (63 to 44 μm), we focused on OSL dating the 4- to 11-μm quartz fraction, which had yielded previously accurate ages (*11*, *13*). Samples for optical dating were taken by hammering 10- to 12-cm-long, 2.6-cm copper tubing into profile walls at close vertical intervals (Figs. 1 to 3). Under safe-light conditions (Na-vapor indirect illumination) in the Geoluminescence Dating

Research Laboratory at Baylor University, the outermost 1.0-cm length of sediment inside the tube was removed, leaving an interior segment with zero ambient light exposure and which was acceptable for OSL dating. Organic matter and carbonate content were removed from the sample by soaking in H_20_2 for 24 hours and reaction with HCl (12%), respectively. Fine-grained (4 to 11 μm) quartz was extracted by suspension settling, following Stokes' law. Subsequently, quartz grains for this fine fraction (4 to 11 μm) were isolated by digestion in hydrofluorosilicic acid (with prior silica saturation) for 6 days (*34*). The mineralogical purity of this fine-grained fraction was checked by an assay with a Raman spectrometer, with a 1-μm beam width. The optical purity of quartz separates was tested by exposing aliquots to infrared excitation (1.08 W from a laser diode at 845 ± 4 nm), which preferentially excites feldspar minerals. If these tests indicated feldspar contamination, then the hydrofluorosilicic acid soaking was repeated. All resultant samples showed weak emissions (<400 counts/s) with infrared excitation at or close to background counts, and the ratio of emissions from blue to infrared excitation of >20, indicating a spectrally pure quartz extract (*35*).

Single aliquot regeneration (SAR) protocols (*36*, *37*) were used in this study to estimate the equivalent dose (D_e). This analysis was completed on the quartz fraction (4 to 11 μm) for 32 sediment samples and for 30 to 50 separate aliquots for each sample (tables S1 and S2). In the laboratory, the sediment was adhered to a 1-cm-diameter circular aluminum disc as a thin coating (<20 μm). This thin layer of sediment was achieved by suspending the fine quartz in methanol (1 cm^3) within a 2-cm^3 flat-bottom tube, with an aluminum disc at the tube bottom. The evaporation of the methanol over 2 to 3 days in total darkness results in the fine-grained fraction adhering to the disc.

An Automated Risø TL/OSL-DA-15 system (*38*) was used for SAR analyses. Blue light excitation (470 ± 20 nm) was from an array of 30 light-emitting diodes that deliver ~15 mW/cm^2 to the sample position at 90% power. Optical stimulation for all samples was completed at an elevated temperature (125°C) using a heating rate of 5°C/s. All SAR emissions were integrated for the first 0.8 s of stimulation out of 40 s of measurement, with background emissions integrated for the last 10 s of data collection, for the 30- to 40-s interval. The luminescence emission for all quartz fractions showed a dominance of a fast component [see (*36*)] with >90% diminution of luminescence after 4 s of excitation (fig. S2), with blue light and with corresponding "fast ratio" of >20 (*39*).

A series of experiments was performed to evaluate the effect of preheating at 160°, 170°, 180°, 190°, 200°, 210°, 220°, 240°, and 260°C on isolating the most robust time-sensitive emissions and thermal transfer of the regenerative signal before the application of SAR dating protocols [fig. S3; see *36*, *37*)]. These experiments entailed giving a known dose (2 to 10 Gy and 31 Gy) and evaluating which preheat temperature resulted in recovery of this dose. There was concordance (±10%) with the known dose for preheat temperatures between 160° and 200°C with a used initial preheat temperature of 180°C for 10 s in the SAR protocols (fig. S3). A second preheat at 180°C for 10 s was applied prior to the measurement of the test dose. A final heating (hot wash) at 260°C for 40 s was applied to minimize carryover of luminescence to the succession of regenerative doses for the equivalent dose analyses (table S1 and fig. S3). A test for dose reproducibility was also performed following procedures of (*36*) with the initial and final regenerative dose of 4.2 Gy (fig. S2), with the resultant recycling ratio of 1.00 ± 0.05.

The SAR protocols were used to resolve equivalent dose for 32 samples (table S1). The statistical significance of an equivalent dose population was determined for 27 to 45 quartz aliquot per sample (table S1). Aliquots were removed from the analysis if the recycling ratio was not between 0.90 and 1.10, the zero dose was >5% of the natural emissions, or the error in equivalent dose determination was >10%. D_e distributions were log normal and exhibited overdispersion values ≤20%, except for sample DF16-05 (table S1 and figs. S1 and S2). An overdispersion percentage of a D_e distribution is an estimate of the relative SD from a central D_e value in the context of a statistical estimate of errors (*40*, *41*). A zero overdispersion percentage indicates high internal consistency in D_e values with 95% of the D_e values within 2σ errors. Overdispersion values <20% are routinely assessed for small aliquots of quartz grains that are well solar reset, such as far-traveled eolian and fluvial sands [e.g., (*42*, *43*)], and this value is considered a threshold metric for calculation of a D_e value using the central age model in (*41*).

The determination of the environmental dose rate is a needed component to calculate an optical age. The dose rate is an estimate of exposure to ionizing radiation for the dated quartz grains. This value is computed from the content of U and Th, ^{40}K, Rb, and cosmic radiation during the burial period (table S1). The U and Th content of the sediments, assuming secular equilibrium in the decay series, ^{40}K, and Rb, was determined by inductively coupled plasma mass spectrometry by ALS Laboratories (Reno, NV). A significant cosmic ray component between 0.24 and 0.29 mGy/year was included in the estimated dose rate, taking into account the current depth of burial (*44*). Moisture content (weight percent) during the burial period was derived from instrumented, nearby pedons whose floodplain soils were similar to those that formed along a higher-order tributary, such as Buttermilk Creek (*11*). Moisture content for these clay-rich sediments (>50% clay) varied between 30 and 38% with an error of 3%. The datum year for all OSL ages is AD 2000.

Statistical analysis: Bayesian analysis of OSL ages

Most of the OSL ages from the Friedkin site were collected in four vertical sediment columns in 2007, 2008, 2015, and 2016. The 2008 and 2015 columns span the south-north extent of Block A. The 2007 column is in the west part of the block, and column 2016 is in the northeast part of the excavation area (Fig. 1B). In addition, OSL samples were taken from areas of interest that were adjacent to the columns. Figure S1 shows the age estimates with 1 SD error bars for the 2007, 2008, 2015, and 2016 columns. OSL ages from specific depths obtained over multiple years mostly overlap at the 68% confidence intervals. The 2008 and 2015 OSL column of dates are consistently very similar to one another (i.e., similar ages are generated at the same depths). The 2007 column ages are similar to the 2008 and 2015 ages with depth, but there are some discrepancies near the top and base of the 2007 column. The 2016 column of ages yielded ages that are consistently younger than those of the other three columns. This is explained by the upward slope of the deposits reflected in the 2007 column of ages and the downward slope of the deposits in the 2016 OSL record.

Bayesian models were created in OxCal to identify outliers and compute posterior age estimates using a Poisson deposition model (*45*, *46*). An age model was created for the 2007 sequence of ages (fig. S1A and table S2), the combined 2008–2015 ages (fig. S1B and table S2), and the 2016 column of ages (fig. S1C and table S2). All four columns are internally consistent with very good agreement levels. The 2007 column of OSL ages shows agreement indices of 115.4/116.7 (model and overall agreement) with a single outlier (UIC2050). Rerunning

the model with the outlier removed increased the agreement indices to 135.9/136.8. The 2008 and 2015 columns were combined into a single Bayesian age model that resulted in model agreement values of 182.3/185.7 with two outliers (UIC2361 and UIC2349). Removing those outliers produced a model with agreement indices of 239/235.2. This combined model was used to produce interpolated ages at approximately 15-mm intervals. Analysis of the 2016 column produced agreement indices of 187.1/179.8 with no outliers.

SUPPLEMENTARY MATERIALS

Supplementary material for this article is available at http://advances.sciencemag.org/cgi/content/full/4/10/eaat4505/DC1

Supplementary Text

Fig. S1. Bayesian ages of Block A OSL columns.

Fig. S2. Regenerative growth curves and plots of D_e values for six OSL samples.

Fig. S3. Preheat dose recovery test for sample BG4066 that was completed for two initial doses of 8 and 31 Gy.

Fig. S4. Diagnostic Folsom and Clovis artifacts.

Fig. S5. Clovis bifaces.

Fig. S6. Pre-Clovis projectile points.

Fig. S7. Pre-Clovis bifaces.

Fig. S8. Use-wear on pre-Clovis artifacts.

Table S1. OSL ages on 4- to 11-μm quartz grains for sediments from the Debra L. Friedkin site, Texas.

Table S2. Correlation of OSL ages with archaeological horizons.

Table S3. Clovis, Folsom, and Buttermilk Creek Complex bifaces.

References (*47*, *48*)

REFERENCES AND NOTES

1. J. V. Moreno-Mayar, B. A. Potter, L. Vinner, M. Steinrücken, S. Rasmussen, J. Terhorst, J. A. Kamm, A. Albrechtsen, A.-S. Malaspinas, M. Sikora, J. D. Reuther, J. D. Irish, R. S. Malhi, L. Orlando, Y. S. Song, R. Nielsen, D. J. Meltzer, E. Willerslev, Terminal Pleistocene Alaskan genome reveals first founding population of native Americans. *Nature* **553**, 203–207 (2018).
2. C. L. Scheib, L. Hongjie, T. Desai, V. Link, C. Kendall, G. Dewar, P. W. Griffith, A. Mörseburg, J. R. Johnson, A. Potter, S. L. Kerr, P. Endicott, J. Lindo, M. Haber, Y. Xue, C. Tyler-Smith, M. S. Sandhu, J. G. Lorenz, T. D. Randall, Z. Faltyskova, L. Pagani, P. Danecek, T. C. O'Connell, P. Martz, A. S. Boraas, B. F. Byrd, A. Leventhal, R. Cambra, R. Williamson, L. Lessage, B. Holguin, E. Ygnacio-De Soto, J. Rosas, M. Metspalu, J. T. Stock, A. Manica, A. Scally, D. Wegmann, R. S. Malhi, T. Kivisild, Ancient human parallel lineages within North America contributed to a coastal expansion. *Science* **360**, 1024–1027 (2018).
3. T. D. Dillehay, C. Ramírez, M. Pino, M. B. Collins, J. Rossen, J. D. Pino-Navarro, Monte Verde: Seaweed, food, medicine, and the peopling of South America. *Science* **320**, 784–786 (2008).
4. J. J. Halligan, M. R. Waters, A. Perrotti, I. J. Owens, J. M. Feinberg, M. D. Bourne, B. Fenerty, B. Winsborough, D. Carlson, D. C. Fisher, T. W. Stafford Jr., J. S. Dunbar, Pre-Clovis occupation 14,550 years ago at the Page-Ladson site, Florida, and the peopling of the Americas. *Sci. Adv.* **2**, e1600375 (2016).
5. M. T. P. Gilbert, D. L. Jenkins, A. Götherstrom, N. Naveran, J. J. Sanchez, M. Hofreiter, P. F. Thomsen, J. Binladen, T. F. G. Higham, R. M. Yohne II, R. Parr, L. S. Cummings, E. Willerslev, DNA from pre-Clovis human coprolites in Oregon, North America. *Science* **320**, 786–789 (2008).
6. D. J. Joyce, Chronology and new research on the Schaefer mammoth (*Mammuthus primigenius*) site, Kenosha County, Wisconsin, USA. *Quat. Int.* **142–143**, 44–57 (2006).
7. M. R. Waters, T. W. Stafford, The First Americans: A review of the evidence for the late-Pleistocene peopling of the Americas, in *Paleoamerican Odyssey*, K. E. Graf, C. V. Ketron, M. R. Waters, Eds. (Texas A&M Univ. Press, 2014), pp. 541–560.
8. M. R. Waters, T. W. Stafford Jr., H. G. McDonald, C. Gustafson, M. Rasmussen, E. Cappellini, J. V. Olen, D. Szklarczyk, L. J. Jensen, M. T. P. Gilbert, E. Willerslev, Pre-Clovis mastodon hunting 13,800 years ago at the Manis site, Washington. *Science* **334**, 351–353 (2011).
9. D. L. Jenkins, L. G. Davis, T. W. Stafford Jr., P. F. Campos, B. Hockett, G. T. Jones, L. S. Cummings, C. Yost, T. J. Connolly, R. M. Yohe II, S. C. Gibbons, M. Raghavan, M. Rasmussen, J. L. A. Paijmans, M. Hofreiter, B. M. Kemp, J. L. Barta, C. Monroe, M. T. P. Gilbert, E. Willerslev, Clovis age Western Stemmed projectile points and human coprolites at the Paisley Caves. *Science* **337**, 223–228 (2012).
10. C. Beck, G. T. Jones, Clovis and Western Stemmed: Population migration and the meeting of two technologies in the Intermountain West. *Am. Antiq.* **75**, 81–116 (2010).
11. M. R. Waters, S. L. Forman, T. A. Jennings, L. C. Nordt, S. G. Driese, J. M. Feinberg, J. L. Keene, J. Halligan, A. Lindquist, J. Pierson, C. T. Hallmark, M. B. Collins, J. E. Wiederhold, The Buttermilk Creek complex and the origins of Clovis at the Debra L. Friedkin site, Texas. *Science* **331**, 1599–1603 (2011).
12. M. R. Waters, C. D. Pevny, D. L. Carlson, *Clovis Lithic Technology: Investigation of a Stratified Workshop at the Gault Site, Texas* (Texas A&M Univ. Press, 2011).
13. S. L. Forman, M. R. Waters, Optically stimulated luminescence dating and the peopling of the Americas. *PaleoAmerica* **2**, 6–10 (2016).
14. K. Rodrigues, W. J. Rink, M. B. Collins, T. J. Williams, A. Keen-Zebert, G. I. López, OSL ages of the Clovis, Late Paleoindian, and Archaic components at Area 15 of the Gault Site, Central Texas, U.S.A. *J. Archaeol. Sci. Rep.* **7**, 94–103 (2016).
15. T. J. Williams, M. B. Collins, K. Rodrigues, W. J. Rink, N. Velchoff, A. Keen-Zebert, A. Gilmer, C. D. Frederick, S. J. Ayala, E. R. Prewitt, Evidence of an early projectile point technology in North America at the Gault site, Texas, USA. *Sci. Adv.* **4**, eaar5954 (2018).
16. S. G. Driese, L. C. Nordt, M. R. Waters, J. L. Keene, Analysis of site formation history and potential disturbance of stratigraphic context in Vertisols at the Debra L. Friedkin archaeological site in central Texas, USA. *Geoarchaeology* **28**, 221–248 (2013).
17. A. K. Lindquist, J. M. Feinberg, M. R. Waters, Rock magnetic properties of a soil developed on an alluvial deposit at Buttermilk Creek, Texas, USA. *Geochem. Geophys. Geosyst.* **12**, 1–11 (2011).
18. M. B. Collins, Archeology in Central Texas, in *The Prehistory of Texas*, T. K. Perttula, Ed. (Texas A&M Univ. Press, 2004), pp. 101–126.
19. J. Lohse, S. L. Black, L. M. Cholak, Toward an improved Archaic radiocarbon chronology for Central Texas. *Bull. Texas Archeol. Soc.* **85**, 259–287 (2014).
20. M. B. Collins, G. L. Bailey, N. A. Kenmotsu, F. A. Weir, *Wilson-Leonard: An 11,000-year Archeological Record of Hunter-Gatherers in Central Texas* (Studies in Archeology 31, Texas Archaeological Research Laboratory, University of Texas, 1998).
21. J. L. Keene, T. Laughlin, M. R. Waters, poster presented at the 83rd Annual Meeting of the Society for American Archaeology, Washington, D.C., 11 to 15 April 2018.
22. C. B. Bousman, B. W. Baker, and A. C. Kerr, Paleoindian Archeology in Texas, in *The Prehistory of Texas*, T. K. Perttula, Ed. (Texas A&M Univ. Press, 2004), pp. 15–97.
23. T. A. Jennings, A. M. Smallwood, M. R. Waters, Exploring late Paleoindian and early Archaic unfluted lanceolate point classification in the Southern Plains. *North Am. Archaeol.* **36**, 243–265 (2015).
24. T. A. Jennings, M. R. Waters, Pre-Clovis lithic technology at the Debra L. Friedkin site, Texas: Comparisons to Clovis through site-level behavior, technological trait-list, and cladistics analysis. *Am. Antiq.* **79**, 25–44 (2014).
25. E. S. Turner, T. R. Hester, R. L. McReynolds, *Stone Artifacts of Texas Indians* (Taylor Trade Publishing, 2011).
26. J. E. Morrow, S. J. Fiedel, D. L. Johnson, M. Kornfeld, M. Rutledge, W. R. Wood, Pre-Clovis in Texas? A critical assessment of the "Buttermilk Creek Complex". *J. Archaeol. Sci.* **39**, 3677–3682 (2012).
27. P. J. Brantingham, T. A. Surovell, N. A. Waguespack, Modeling post-depositional mixing of archaeological deposits. *J. Anthropol. Archaeol.* **26**, 517–540 (2007).
28. L. G. Davis, A. J. Nyers, S. C. Willis, Context, provenance, and technology of a Western Stemmed Tradition artifact cache from the Cooper's Ferry site, Idaho. *Am. Antiq.* **79**, 596–615 (2014).
29. L. Aveleyra Arroyo de Anda, M. Maldonado-Koerdell, Association of artifacts with mammoth in the Valley of Mexico. *Am. Antiq.* **18**, 332–340 (1953).
30. S. Gonzalez, D. Huddart, I. Israde-Alcántara, G. Domínguez-Vázquez, J. Bischoff, N. Felstead, Paleoindian sites from the Basin of Mexico: Evidence from stratigraphy, tephrochronology and dating. *Quat. Int.* **363**, 4–19 (2015).
31. N. Flegenheimer, L. Miotti, N. Mazzia, Rethinking early objects and landscapes in the Southern Cone: Fishtail-point concentrations in the Pampas and northern Patagonia, in *Paleoamerican Odyssey*, K. E. Graf, C. V. Ketron, M. R. Waters, Eds. (Texas A&M Univ. Press, 2014), pp. 359–376.
32. A. J. Lesnek, J. P. Briner, C. Lindqvist, J. F. Baichtal, T. H. Heaton, Deglaciation of the Pacific coastal corridor directly preceded the human colonization of the Americas. *Sci. Adv.* **4**, eaar5040 (2018).
33. L. G. Davis, S. C. Willis, S. J. Macfarlan, Lithic technology, cultural transmission, and the nature of the Far Western Paleoarchaic/Paleoindian co-tradition, in *Meeting at the Margins*, D. Rhode, Ed. (Univ. Utah Press, 2012), pp. 47–64.
34. S. Stokes, S. Ingram, M. J. Aitken, F. Sirocko, R. Anderson, D. Leuschner, Isolation of silt-sized quartz from sediments. *Ancient TL* **18**, 7–11 (1980).
35. G. A. T. Duller, L. Bøtter-Jensen, A. S. Murray, Combining infrared- and green-laser stimulation sources in single-grain luminescence measurements of feldspar and quartz. *Radiat. Meas.* **37**, 543–550 (2003).
36. A. S. Murray, A. G. Wintle, The single aliquot regenerative dose protocol: Potential for improvements in reliability. *Radiat. Meas.* **37**, 377–381 (2003).
37. A. G. Wintle, A. S. Murray, A review of quartz optically stimulated luminescence characteristics and their relevance in single-aliquot regeneration dating protocols. *Radiat. Meas.* **41**, 369–391 (2006).
38. L. Bøtter-Jensen, E. Bulur, G. A. T. Duller, A. S. Murray, Advances in luminescence instrument systems. *Radiat. Meas.* **32**, 523–528 (2000).

39. J. A. Durcan, G. A. T. Duller, The fast ratio: A rapid measure for testing the dominance of the fast component in the initial OSL signal from quartz. *Radiat. Meas.* **46**, 1065–1072 (2011).
40. R. F. Galbraith, R. G. Roberts, Statistical aspects of equivalent dose and error calculation and display in OSL dating: An overview and some recommendations. *Quat. Geochronol.* **11**, 1–27 (2012).
41. R. F. Galbraith, R. G. Roberts, G. M. Laslett, H. Yoshida, J. M. Olley, Optical dating of single and multiple grains of quartz from Jinmium rock shelter, northern Australia: Part 1, Experimental design and statistical models. *Archaeometry* **41**, 339–364 (1999).
42. J. M. Olley, T. Pietsch, R. G. Roberts, Optical dating of Holocene sediments from a variety of geomorphic settings using single grains of quartz. *Geomorphology* **60**, 337–358 (2004).
43. S. L. Forman, A. Tripaldi, P. L. Ciccioli, Eolian sand sheet deposition in the San Luis paleodune field, western Argentina as an indicator of a semi-arid environment through the Holocene. *Palaeogeogr. Palaeoclimatol. Palaeoecol.* **411**, 122–135 (2014).
44. J. R. Prescott, J. T. Hutton, Cosmic ray contributions to dose rates for luminescence and ESR dating: Large depths and long-term time variations. *Radiat. Meas.* **23**, 497–500 (1994).
45. C. B. Ramsey, Deposition models for chronological records. *Quat. Sci. Rev.* **27**, 42–60 (2008).
46. C. B. Ramsey, OxCal Version 4.2.4. Oxford University (2013); https://c14.arch.ox.ac.uk/oxcal.html.
47. D. A. Suhm, E. B. Jelks, *Handbook of Texas Archaeology: Type Descriptions* (Texas Memorial Museum Bulletin no. 4, 1962).
48. R. F. Galbraith, P. F. Green, Estimating the component ages in a finite mixture. *Int J Rad Appl Instrum A* **17**, 197–206 (1990).

Acknowledgments: We thank Debra and Dan Friedkin for permission to excavate at the site and for field logistical support, R. Lopez and M. Yalch for assistance during the excavation, and T. Stafford and J. Halligan for reviewing the drafts of this manuscript. **Funding:** Funds generated by the North Star Archaeological Research Program Endowment established by J. Cramer and R. Cramer funded most of the fieldwork and analyses conducted at the Friedkin site. Funding from the Elfrieda Frank Foundation supported the 2016 excavations. Laboratory analysis was funded in part by the Chair in First Americans Studies. The open access publishing fees for this article have been covered by the Texas A&M University Open Access to Knowledge Fund (OAKFund), supported by the University Libraries and the Office of the Vice President for Research. **Author contributions:** M.R.W. and J.L.K. conducted the excavations and artifact analysis and wrote the paper. S.L.F. conducted the OSL dating and wrote the corresponding supplemental section. E.R.P. identified and described all the projectile points from the Friedkin site. D.L.C. conducted the Bayesian analysis and wrote the corresponding supplemental section. J.E.W. conducted the artifact use-wear analysis and wrote the corresponding supplemental section. All authors reviewed the final draft. **Competing interests:** All authors declare that they have no competing interests. **Data and materials availability:** All data needed to evaluate the conclusions in the paper are present in the paper and/or the Supplementary Materials. Additional data related to this paper may be requested from the authors.

Submitted 27 February 2018
Accepted 19 September 2018
Published 24 October 2018
10.1126/sciadv.aat4505

Citation: M. R. Waters, J. L. Keene, S. L. Forman, E. R. Prewitt, D. L. Carlson, J. E. Wiederhold, Pre-Clovis projectile points at the Debra L. Friedkin site, Texas—Implications for the Late Pleistocene peopling of the Americas. *Sci. Adv.* **4**, eaat4505 (2018).

Pre-Clovis projectile points at the Debra L. Friedkin site, Texas—Implications for the Late Pleistocene peopling of the Americas

Michael R. Waters, Joshua L. Keene, Steven L. Forman, Elton R. Prewitt, David L. Carlson and James E. Wiederhold

Sci Adv **4** (10), eaat4505.
DOI: 10.1126/sciadv.aat4505

Science Advances
AAAS

advances.sciencemag.org/cgi/content/full/4/10/eaat4505/DC1

Supplementary Materials for

Pre-Clovis projectile points at the Debra L. Friedkin site, Texas—Implications for the Late Pleistocene peopling of the Americas

Michael R. Waters*, Joshua L. Keene, Steven L. Forman, Elton R. Prewitt, David L. Carlson, James E. Wiederhold

*Corresponding author. Email: mwaters@tamu.edu

Published 24 October 2018, *Sci. Adv.* **4**, eaat4505 (2018)
DOI: 10.1126/sciadv.aat4505

This PDF file includes:

SUPPLEMENTARY TEXT

Projectile Point Identification and Descriptions

Type names for projectile points were determined by recording the attributes of each point and then comparing these to the attributes of known point types from other excavated sites. Late Prehistoric and Archaic projectile points follow the type names in (*47*). Paleoindian projectile points follow the types defined in (*20*). The Texas point identification guide (*25*) is used as a secondary source for identifications. All Buttermilk Creek Complex triangular lanceolate and stemmed lanceolate projectile points and point fragments discussed in the main text are described in detail.

Triangular Lanceolate Projectile Point

AM9811-1. This triangular point (Fig. 5A; fig. S6A) lacks the distal tip due to a diagonal snap fracture that probably resulted from impact. The remaining lateral blade edges are gently concave although they are somewhat irregular. They are alternately beveled to the right at 45º to 50º. The blade was resharpened at least once before the piece was discarded. The long haft element has essentially straight lateral edges, but as with the blade they are somewhat irregular. The haft is defined by very light grinding along the lateral edges. The gently concave base also exhibits very light grinding. The base is thinned on one face by a flute-like flake that extends upward slightly diagonal left about 22 mm. An apparent attempt to remove a similar flake from the opposite face terminated in a hinge fracture that left an unremoved knot on that face.

Lanceolate Stemmed Projectile Points

AM9875-2. The leaf-shaped blade of this lanceolate point (Fig. 5B; fig. S6B) has convex lateral edges that are gently (40º) alternately beveled to the left. A small segment of the distal tip is absent due to a snap fracture. The weak, but distinct, shoulders transition to a gently contracting stem with gently concave lateral edges that are heavily ground. Although one ear of the stem is absent, the slightly concave base exhibits light grinding. Due to its concave lateral edges, the stem expands very slightly at the base. The base was thinned by removing multiple short flakes from each face. On one face, the flaking pattern is generally sub-parallel although a small portion on the upper right appears random. The sub-parallel pattern includes the stem as well as the blade. On the opposite face, including the stem, the flaking pattern is oblique sub-parallel extending from upper left to lower right. Most of the final margin trimming flakes occur on this face.

AM8286-16. Base fragment of large stemmed point (Fig. 5G; fig. S6H) that was broken by a snap fracture, likely while in the haft. Subtle shoulders define the boundary between the blade and stem. The edges of the stem contract and are straight. The base is also straight. The edges and base of the stem are lightly ground. The blade gently expands outward from the base and is alternately beveled at 45º. The base was shaped by percussion flaking and is thickest in the midsection.

AM6233-1: The blade of this medial segment of a lanceolate point (Fig. 5D; fig. S6G) has been resharpened. The straight lateral edges of the blade are alternately beveled to the right at 55º. The distal tip is absent due to a snap fracture. The piece is widest at the shoulders formed by the juncture of the blade and the stem or haft element. The straight lateral edges of the slightly

contracting stem are heavily ground. The base is absent; burin-like blows from either corner removed any vestige of the base.

AM12017-1: This is a medial fragment of a lanceolate point (Fig. 5C; fig. S6E). The extant segment of the blade has been resharpened. The lateral edges are straight and both are moderately beveled on the same face, 55º to left and 45º to right. The shoulders are the widest part of the blade at the juncture of the blade and stem. The distal blade portion is missing due to a snap fracture. The stem contracts very slightly; the lateral edges are essentially straight and are moderately ground. The base is absent due to a snap fracture. This piece is quite similar to specimens AM6233-1 and AM11385-1.

AM12271-1: This piece consists of a medial fragment at the juncture of the blade and stem of a lanceolate point (Fig. 5E; fig. S6K). The blade exhibits straight lateral edges that are gently (40º) alternately beveled to the right. Shoulders are absent. The stem remnant is too short to characterize its lateral edges other than that they are lightly ground. The distal tip and the base both are absent due to snap fractures. The flake patterns on one face are slightly diagonal upper left to lower right and are sub-parallel. A similar pattern exists on the opposite face, but in this instance angle from upper right to lower left. This fragment appears to be very similar to specimens AM6233-1 and AM12017-1.

AM4819-7: This is a medial fragment at the juncture of the blade and stem (Fig. 5H; fig. S6F). This specimen has been heavily damaged, likely as a result of impact. What is clear is that the blade is indented relative to the base and shows alternate bevels of 55 º on both sides.

AM8380-3: This very short distal fragment of a point (Fig. 5J; fig. S6D) has straight lateral edges that are alternately moderately beveled (55º) to the right. It was separated from the parent point by an impact fracture.

AM12029-2: This very small rectangular medial point fragment (Fig. 5K; fig. S6C) retains one apparent lateral edge segment that is beveled at 65º. There are snap fractures on both distal and proximal ends. It is probable that this piece represents a small segment of a beveled projectile point blade.

AM12170-1: While technically a medial fragment due to the very distal tip having been removed by an impact fracture, this distal segment of a point (Fig. 5I; fig. S6L) is relatively narrow. It exhibits essentially straight lateral edges that are alternately strongly beveled (65º) to the right. It is too fragmentary to determine the full original blade characteristics. The original flake patterns on one face are oblique sub-parallel extending from lower left to upper right while those on the opposite face are oblique sub-parallel but extend upper left to lower right. This piece was detached from the proximal point elements by an indeterminate fracture.

AM12274-13: This thin distal point fragment (Fig. 5L; fig. S6J) has essentially straight lateral edges that are not beveled. The piece was detached from the parent point by a snap fracture. Flake patterns on one face are sub-parallel while those on the opposite face are oblique sub-parallel extending from upper right to lower left.

AM4668-6: This is the distal portion of a lanceolate point (Fig. 5F; fig. S6I). The blade is lightly alternately beveled at angles of 40º and 50º and was broken by a snap fracture.

Diagnostic aspects of the lanceolate stemmed projectile points are the beveled blades and the gently contracting stems. The complete specimen AM9875-2 appears to have been lightly resharpened, yet it is very gently alternately beveled indicating that this was an intentional blade edge treatment. All but one specimen exhibits beveled blades. Most are beveled on alternate faces. The indented nature of the blade relative to the base suggests in-haft blade refurbishment was a common practice. The one complete point, base fragment, and medial fragments show that these points had stemmed bases that are ground. This assemblage is remarkably consistent with beveled blades and gently contracting stems.

Artifact Use-Wear Analysis

Use-wear studies were conducted at the Center for the Study of the First Americans using a Leica DMLA compound microscope fitted with Nomarski optics to observe use-wear characteristics at magnifications of 100X, 200X, and 500X. Images were recorded with a CoolSnapPro camera integrated with Image-Pro Plus software to produce a clear focused image at high magnification (fig. S8). Artifacts were cleaned with a mild detergent and sonication. Alcohol on a cotton swab was used to periodically to remove oils and grease. Microscopic use-wear on six Buttermilk Creek Complex projectile points and point fragments is described.

AM9875-2 is a lanceolate stemmed point with use-wear characteristics that suggest the artifact was used as a hafted projectile point. Use-wear is shown at three locations (fig. S8, 1A-1C). The 1A images show polish developed on an arris between flake scars. The image at 100X shows polish on three locations. In the center of the image, polish is seen on the ridge between two large scars that were likely formed from manufacture. To the right of this ridge and nearer the edge, polish has formed on a step-fracture termination and is oriented parallel to the edge. At the bottom left of the image, polish can be seen on the ridge of a small flake scar on the immediate edge. Images at 200X and 500X show the larger flake scar ridge having well-developed polish and patterned striae trending nearly parallel to the edge. The 1B images show a high, flat facet adjacent to the break at the distal tip nearly covered by a moderately-developed polish containing light striae that are oriented parallel to the long axis of the point. The 1C images are from a topographically high area within the haft element, where only the very highest areas exhibit polish. This polish is well-developed and flattens the micro-topography of the material. The polish contains groups of light, randomly-oriented striae. These attributes imply a rigid contact material and slight but sustained movement, which along with their location, indicate haft wear.

AM8286-16 is a lanceolate stemmed point base with three locations of use-wear depicted (fig. S8, 2A-2C). Although the distal working end of this artifact is missing, the documented use-wear characteristics strongly suggest that this artifact was used as a hafted projectile point and knife. The 2A images were captured near the junction of two flake scar ridges, an area of the highest relief on this face. The polish in these images is confined to the peak of the ridge and is very well-developed in the flattened area seen at the center of the image. Short multi-directional striae are visible at 200X and 500X. These characteristics suggest slight and repeated movement against a rigid haft material over a significant amount of time. The 2B images show a series of ridges at the first high topographic area from the proximal end of the artifact. As the two images show, polish has developed on these ridges and is largely confined there. However, due to the formation and angle of the ridges, the polish has expanded to a wider area as seen at 200X and 500X. At 500X, short multi-directional striae can be seen. These features also indicate that this artifact spent a substantial amount of time in a haft. The 2C images show two flake scars and the

arris between them near the distal, broken end of the artifact. This location is distal to the hafted portion of the artifact. There are small, scattered areas of polish development on high areas around the flake scars seen at 200X. At 500X, polish and micro-flaking are visible on the extreme edge of the piece between the flake scars.

AM12017-1 is a lanceolate stemmed point midsection with a partial base and blade. Use-wear is shown at two locations (figs. S8, 3A-3B). Documented use-wear characteristics strongly suggest this artifact was used for thrusting or as a projectile. The 3A images show a worn step-fracture termination with polish on the highest and most interior step. This polish is heaviest close to the edge and is beginning to show linkage and its directionality appears to be perpendicular to the edge. The 500X image shows linkage but little flattening of the micro-topography. These characteristics suggest a moderate amount of haft wear. The 3B images show a diffuse, fairly weak polish on a flat interior surface which is consistent on the interior surfaces of both sides. At 500X some linkage can be seen developing and short randomly oriented striae are also visible. This example is some of the heaviest wear on the artifact. The use-wear on AM12017-1 implies repeated use as a hafted projectile that likely sustained forceful thrusts into an abrasive, but yielding material such as soil, before breakage.

AM12170-1 is a projectile point tip fragment with use-wear shown in two locations (fig. S8, 4A-4B). The use-wear on this tip is consistent with projectile point use. The 4A images show well-developed polish confined to an area of high topographic relief and clearly showing that the force producing the wear came from the distal end. At 500X the polish has altered the micro-topography to the extent that it appears nearly flat. Short striae are visible parallel to the long axis of the tip indicating direction of use. The 4B images came from a ridge on the same edge of the artifact and show polish forming on the leading edge of a high-relief area.

AM4668-6 is a projectile point tip fragment with use-wear shown in three locations (fig. S8, 5A-5B) The use-wear on this artifact is compatible with use as a projectile point. The 5A images show extensive polish on a high area at the extreme distal tip. The polish has a linear appearance that is parallel to the long axis of the artifact produced by a thrusting motion. The 5B images near the snapped end show alternate streaks of polished and non-polished surface. These linear indicators are parallel to the long axis of the artifact.

AM9811-1 is a triangular lanceolate point with use-wear shown at five locations (fig. S8, 6A-6C). Documented use-wear is consistent with use as a projectile point and knife. The 6A images come from a flat raised area with extensive polish that apparently formed before the break occurred. As expected with use a projectile, the polish is heavier toward the distal end and becomes less developed farther away from the distal end. At 200X and 500X, striae can be seen trending both parallel and oblique to the long axis of the point. The 6B images show a well-developed polish on a flake scar ridge that is situated oblique to the long axis. The polish and striae shown here indicate a longitudinal direction of tool movement that is consistent with use as a projectile point. Along the broken edge, the 6C images are from the haft area on the opposite face and also show polish on a flake scar ridge.

SUPPLEMENTAL FIGURES AND TABLES

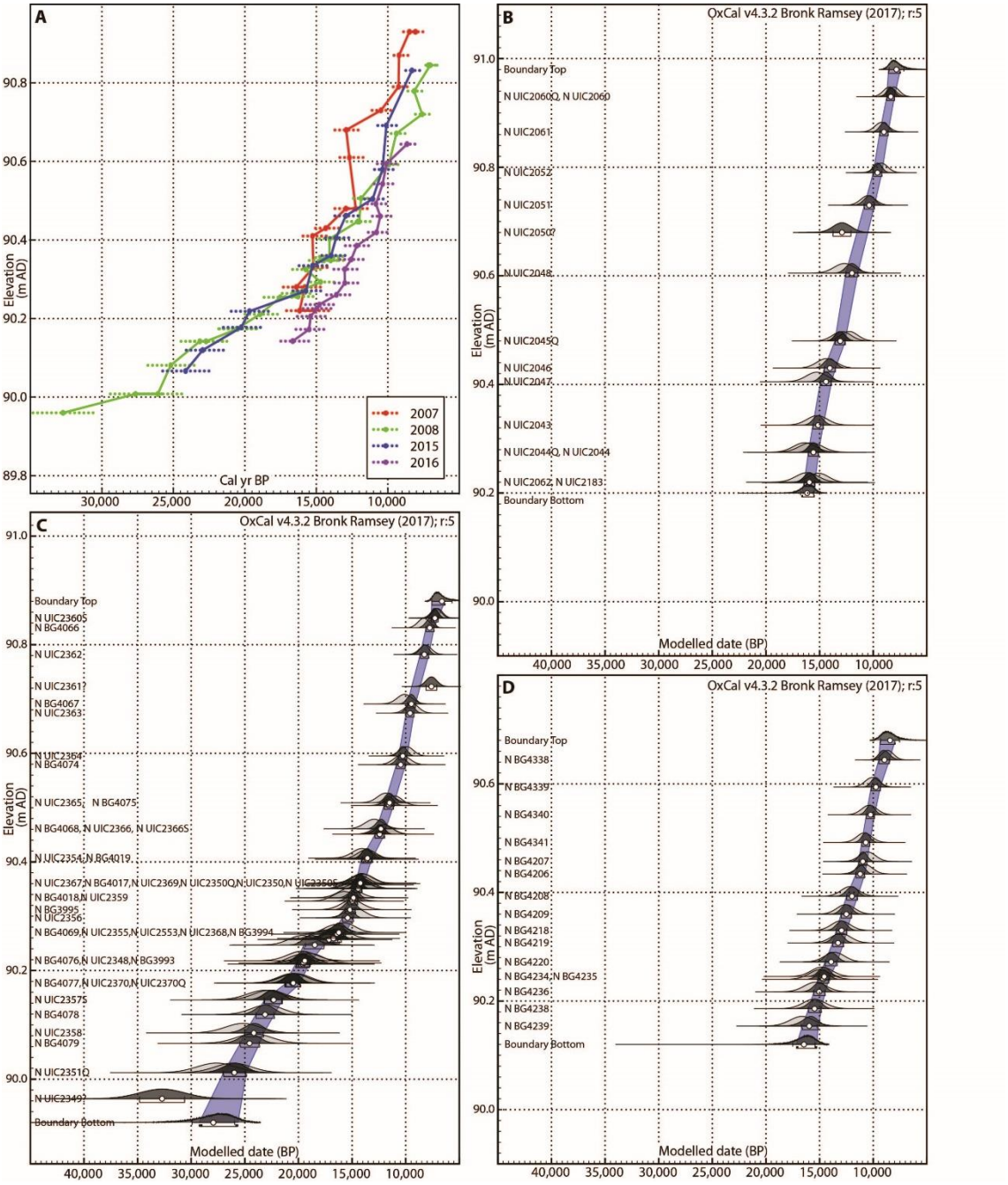

Fig. S1. Bayesian ages of Block A OSL columns. (A) Plot of OSL ages from the 2007, 2008, 2015, and 2016 columns with depth in m AD. A solid dot indicates an OSL date mean and the dotted line to the left and right indicates the standard deviation of the age at one sigma. (B) Bayesian analysis of the 2007 OSL ages. One age outlier is identified and not used in the age model. (C) Bayesian analysis of combined OSL ages from 2008 and 2015. Two outliers identified and were not used in the age model. (D) Bayesian analysis of the 2016 OSL ages.

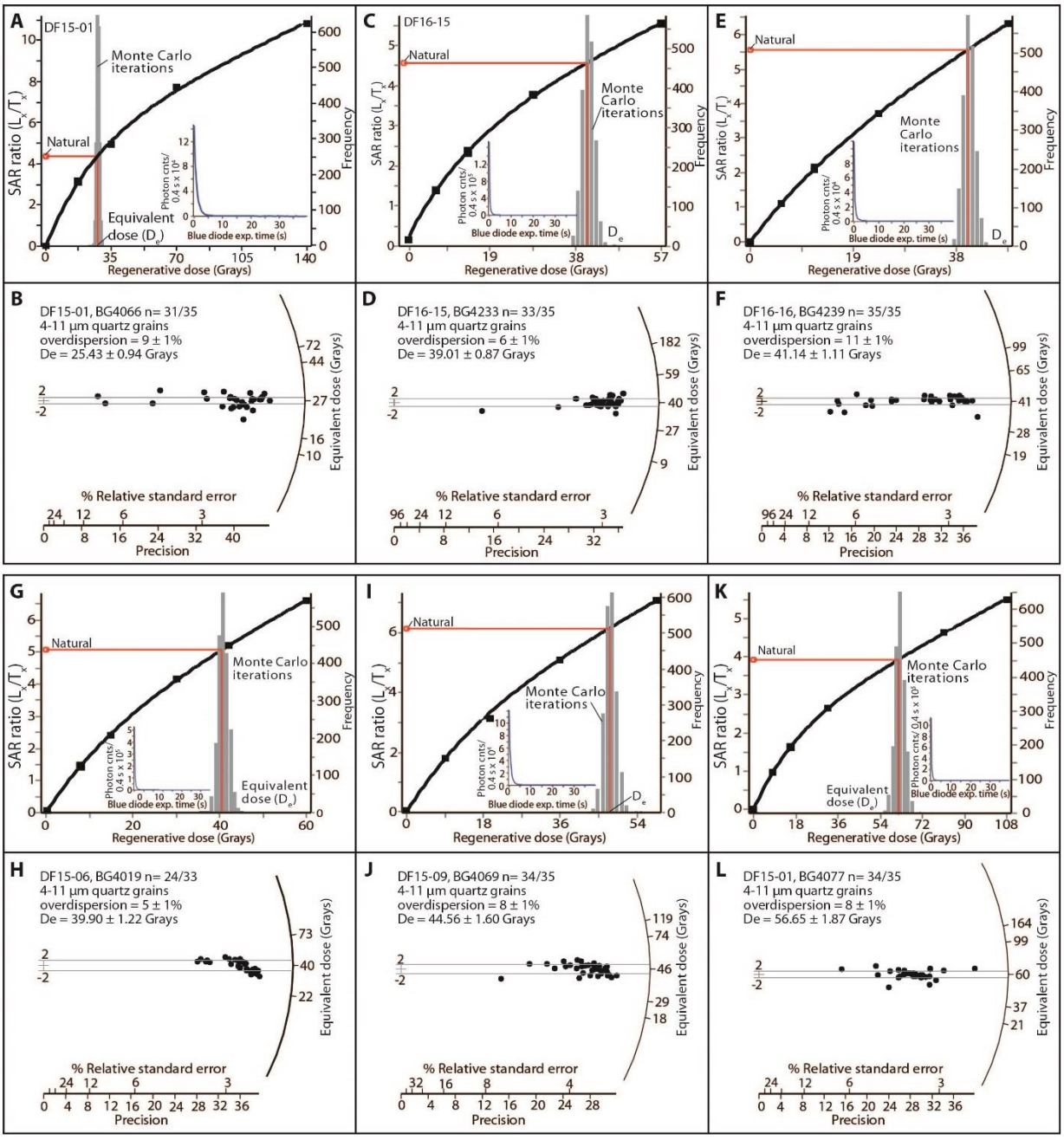

Fig. S2. Regenerative growth curves and plots of D_e values for six OSL samples. (A, C, E, G, I, K) Regenerative growth curve for quartz grains from the Friedkin site showing Monte Carlo iterations to resolve an equivalent dose (De) for six different samples (BG4066, BG4238, BG4239, BG4019, BG4069, BG4077). Inset figure shows OSL shine-down curve. (B, D, F, H, J, L) Radial plots of equivalent dose (De) values on aliquots for same six samples. Shown are the two sigma De range for central age model (after *40*).

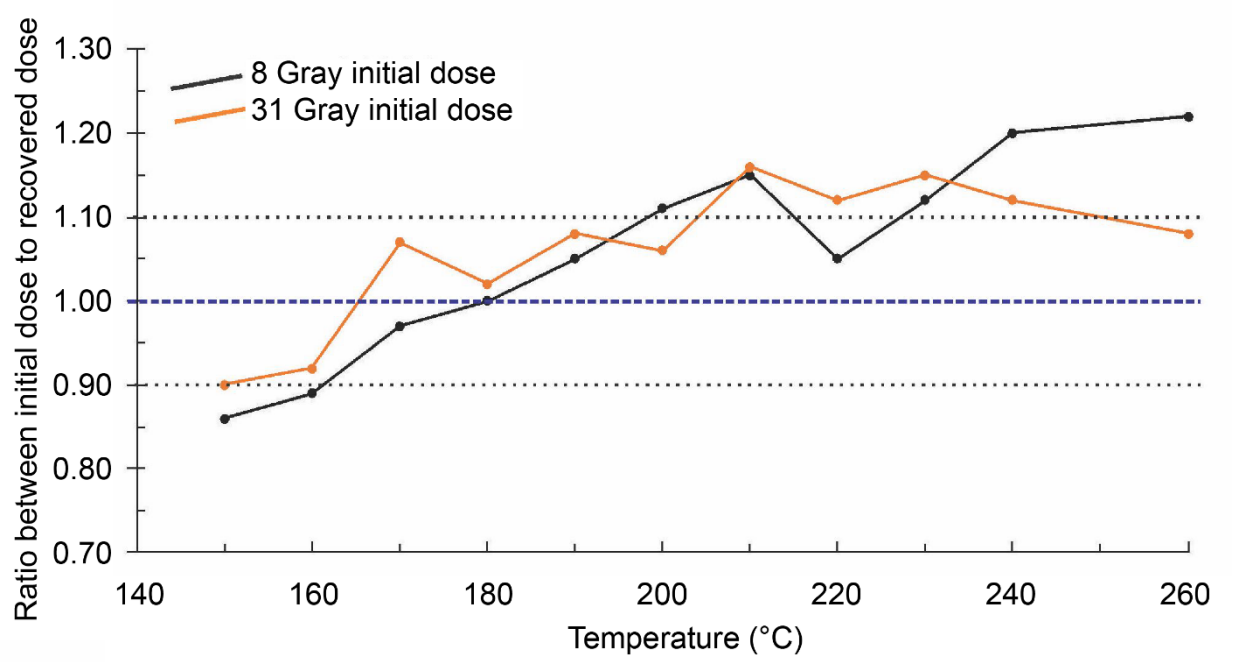

Fig. S3. Preheat dose recovery test for sample BG4066 that was completed for two initial doses of 8 and 31 Gy. The desired preheat yields a ratio of 1.0 ± 0.1 which reflects agreement within in 10% of the initial dose and recovered dose. We choose a preheat temperature of 180° C because this temperature through many tests yielded a unity ratio within 5%. Each point in the graph by temperature reflects the average of 3 analyses, with combined errors of 0.02-0.05.

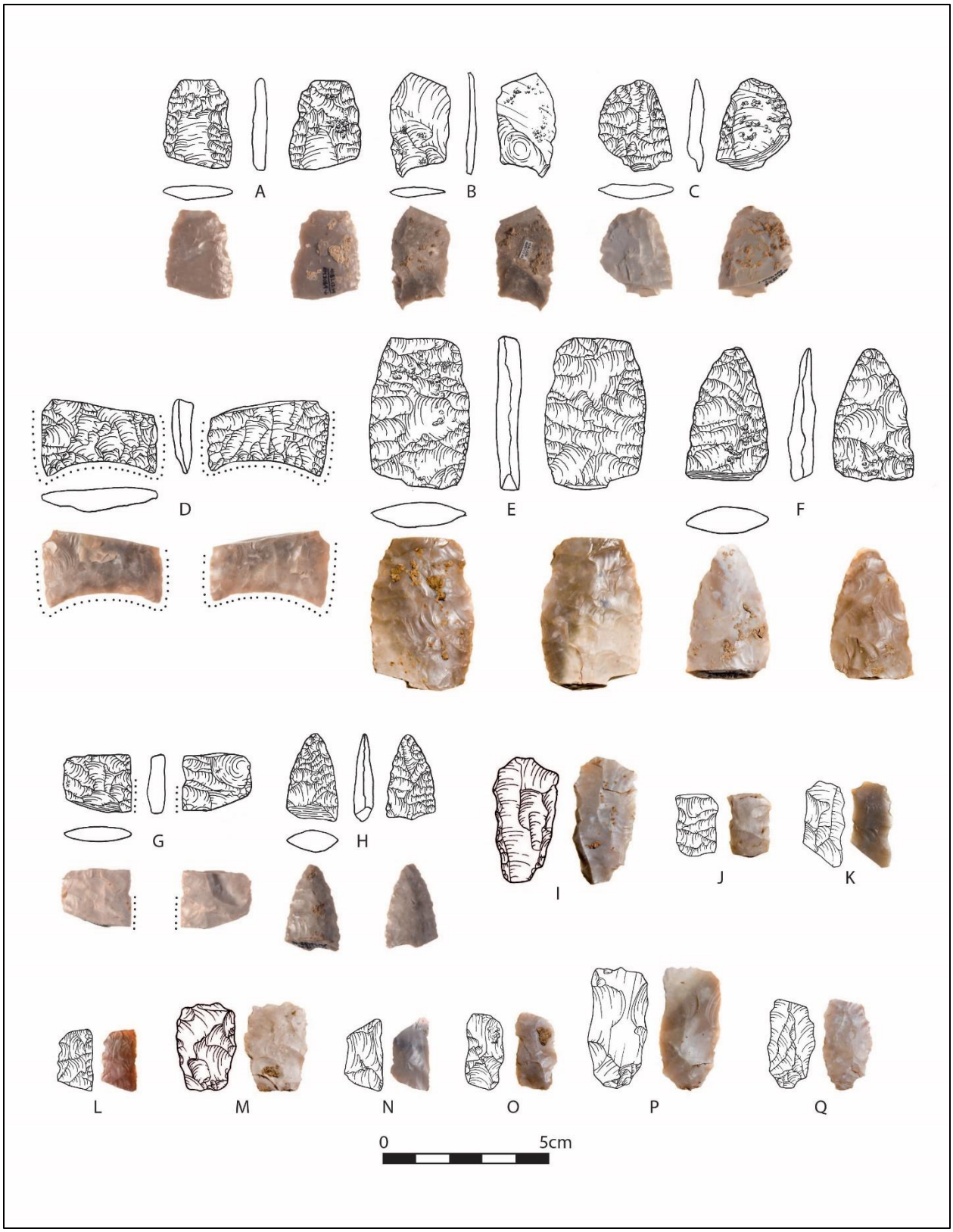

Fig. S4. Diagnostic Folsom and Clovis artifacts. Diagnostic Folsom artifacts: (A) AM3069-6 is a Folsom point that is fluted on both sides and has been reworked; (B) AM9717-43 represents a fluting failure. The point split in half with a remnant of the base preserved on both faces; (C)

AM4525-1 is a fluting failure. During final fluting, the preform snapped. Clovis projectile points. (D) AM12018-1 base of Clovis point. Use-wear studies show evidence of hafting; (E) AM4581-7 midsection of Clovis point. Use-wear studies show evidence of striations and polish consistent with use as a projectile; (F) AM4871-6 tip of Clovis point with use-wear; (G) AM4447-1 midsection of a Clovis point with terminal flute scars on both faces. Basal edge is ground. (H) AM3138-4 tip of a Clovis point with use-wear. Dots indicate areas of grinding in the hafted portion of the point. Channel or flute flakes: (I) AM3164-2; (J) AM5808-5; (K) AM6135-10; (L) AM8224-4; (M) AM9763-19; (N) AM9732-10; (O) AM9679-8; (P) AM9767-6; (Q) AM9797-7.

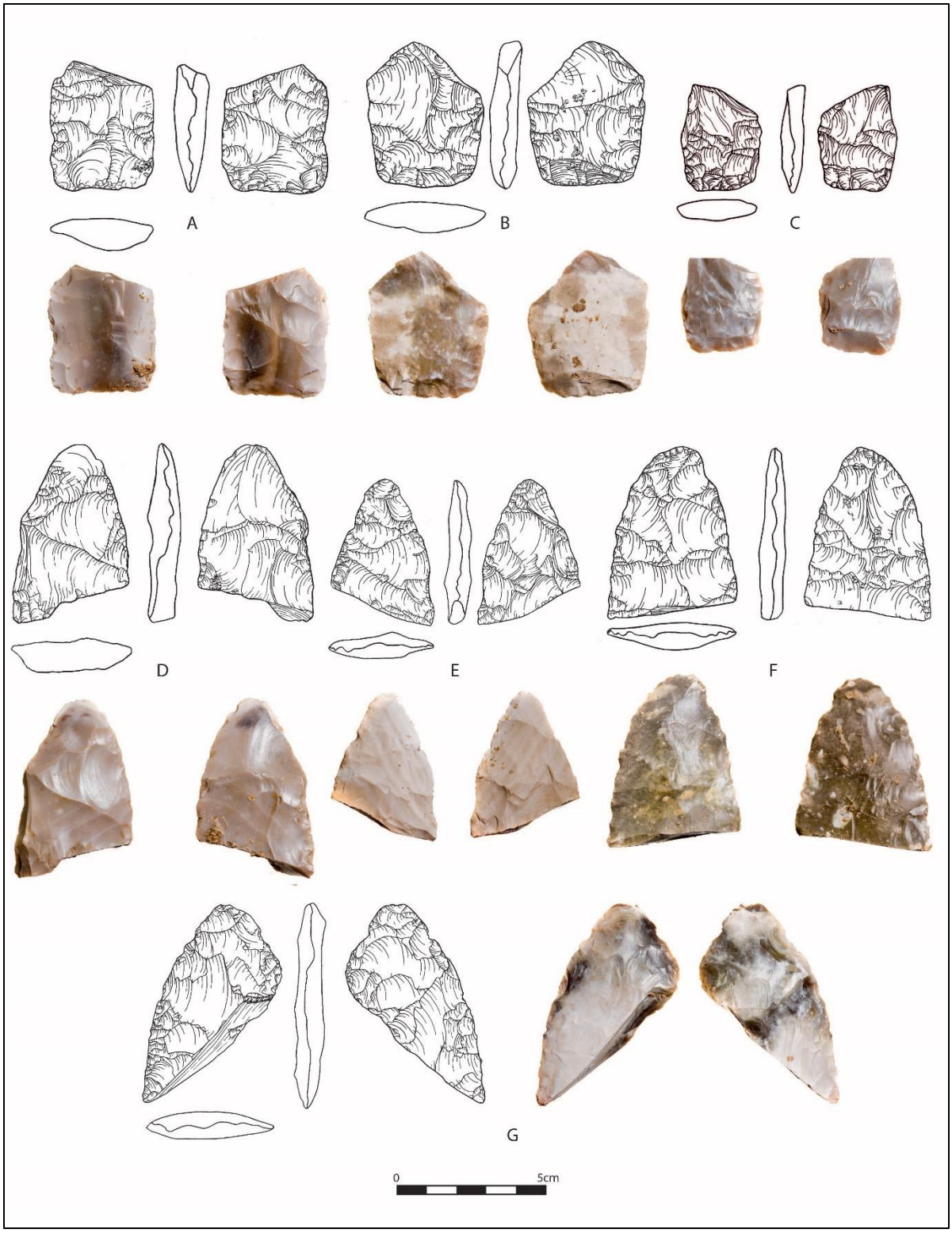

Fig. S5. Clovis bifaces. Shown is a selection of representative Clovis bifaces. (A) AM6093-5 basal biface with endthinning; (B) AM11851-9 basal biface with overface flake scars and beveled base; (C) AM9731-7 basal biface with distinct bevel and overface and overshot flake scars; (D) AM8122-1 distal biface with overface and overshot flake scars; (E) AM5842-7 distal biface with overface and overshot flake scars; (F) AM12010-1 distal biface with overface flake scars; (G) AM12262-19 distal biface with overface flake scars.

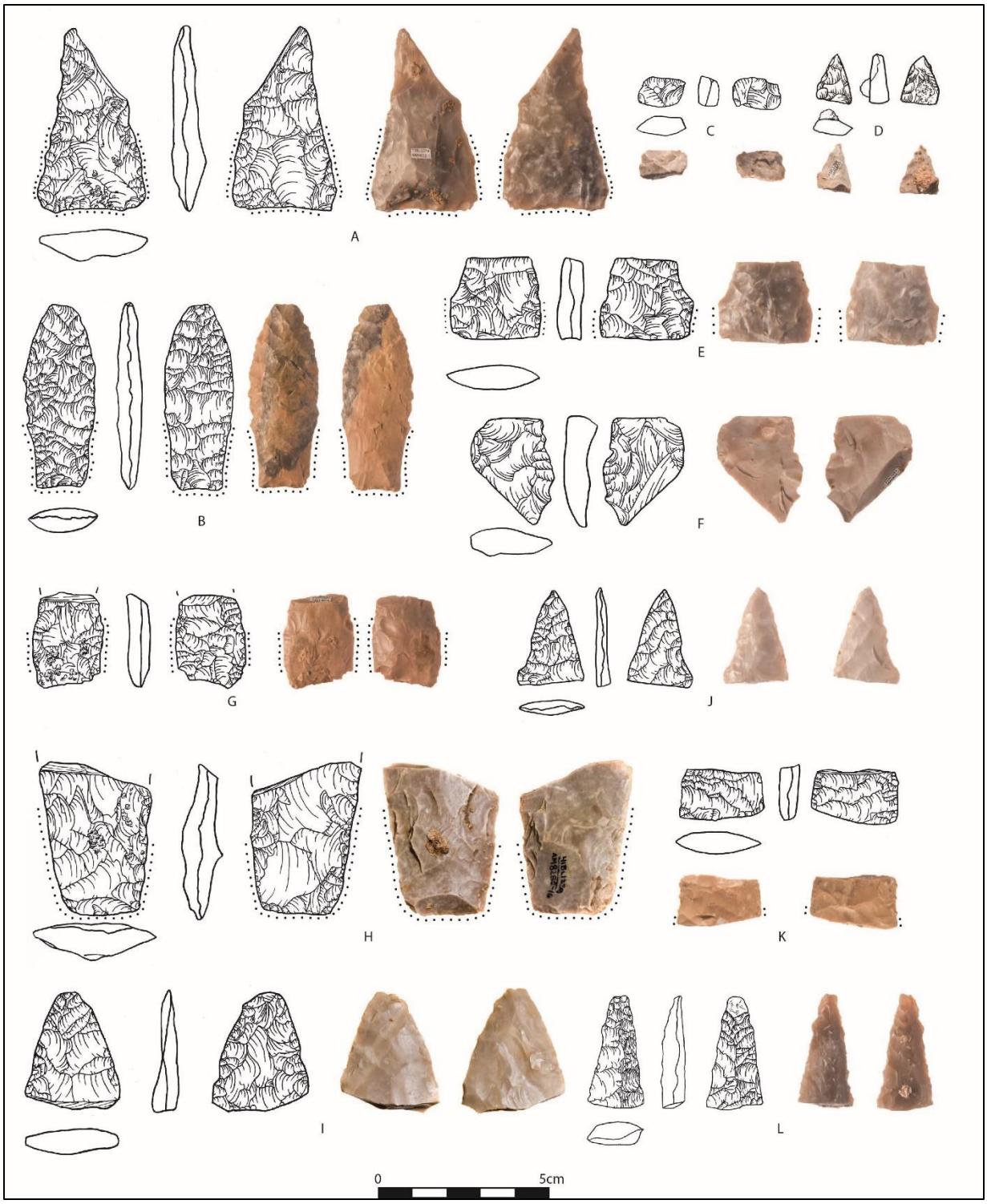

Fig. S6. Pre-Clovis projectile points. (A) AM9811-1 triangular lanceolate point with basal flute-like end thinning scars; (B) AM9875-2 lanceolate stemmed point; (C) AM12029-2 midsection of a beveled tip similar to AM12170-1; (D) AM8380-3 beveled tip similar to AM12170-1; (E) AM12017-1 lanceolate stemmed point midsection with both base and blade segments; (F) AM4819-7 lanceolate stemmed point midsection heavily damaged from impact; (G) AM6233-1 midsection of lanceolate stemmed point with base and blade segments; (H)

AM8286-16 base fragment of lanceolate stemmed point; (I) AM4668-6 tip of projectile point; (J) AM12274-13 tip of projectile point; (K) AM12271-1 midsection of lanceolate stemmed point with base and blade segments; (L) AM12170-1 beveled tip. Dots indicate areas of grinding in the hafted portion of the point.

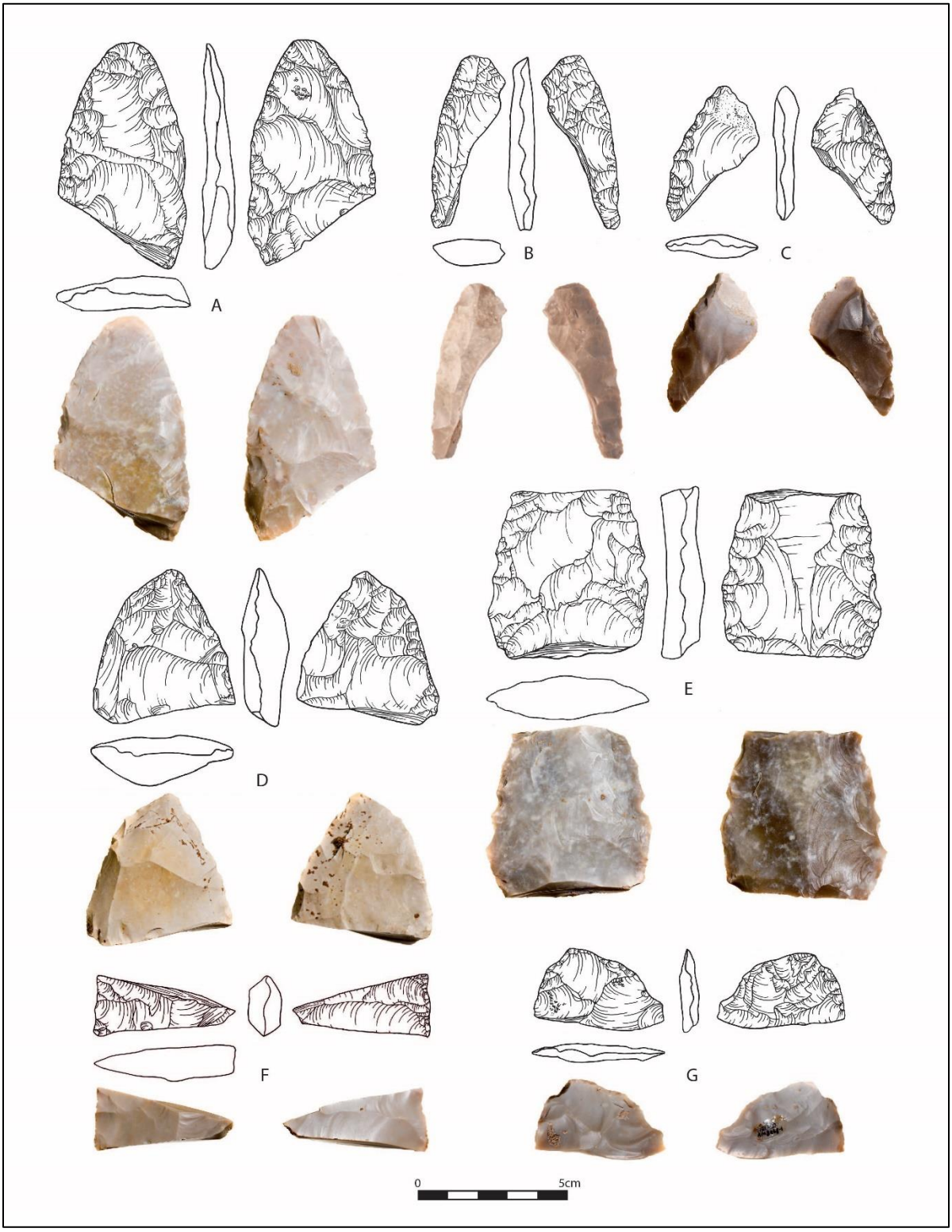

Fig. S7. Pre-Clovis bifaces. Shown is a selection of representative Buttermilk Creek Complex bifaces. (A) AM9855-1 distal biface with overface flake scars; (B) AM4777-2 biface preform; (C) AM12125-7 distal biface. (D) AM3277-1 distal biface; (E) 12085-1 midsection of biface; (F) AM8256-2 midsection of biface with overface flake scars; (G) AM8408-1 distal biface.

Fig. S8. Use-wear on pre-Clovis artifacts. AM9875-2: Lanceolate stemmed point showing use-wear at locations 1A-1C at 200x and 500x. Use-wear characteristics indicate use as a hafted projectile point. AM8286-16: Lanceolate stemmed point base showing use-wear documented at

locations 2A-2C at 200x and 500x. Although the distal working end of this artifact is missing, the documented use-wear characteristics show that this artifact was used as a hafted projectile point and knife. AM12017-1: Images of use-wear on lanceolate stemmed point midsection with base and blade at locations 3A-3B at 200x and 500x. The use-wear shows both haft and projectile wear. AM12170-1: Tip fragment showing the locations of use-wear at points 4A-4B at 200x and 500x, which likely was produced by projectile use. AM4668-6: Images of use-wear documented at locations 5A-5B at 200x and 500x, showing use as a projectile. AM9811-1: Use-wear documented at localities 6A-6B at 200x and 500x, and 6C at 100x, 200x, and 500x on a triangular lanceolate point. Use-wear indicates that the artifact was hafted and used as a projectile point. Labels marked with * indicate use-wear on opposite face.

Table S1. OSL ages on 4- to 11-µm quartz grains for sediments from the Debra L. Friedkin site, Texas.

Sample	Depth (m. AD)	Laboratory Number	Aliquots†	Equivalent dose (Gray)‡	Over-Dispersion (%)§	Alpha Efficiency	U (ppm)‖	Th (ppm)‖	K (%)‖	H_20 (%)	Cosmic dose (mGray/yr)¶	Dose rate (mGray/yr)¶	OSL age (yr B.P.) #
DF15-01	90.831	BG4066	31/35	25.43 ± 0.94	9 ± 1	0.08 ± 0.01	2.92 ± 0.01	13.30 ± 0.01	1.10 ± 0.01	30 ± 3	0.202 ± 0.020	3.06 ± 0.15	8315 ± 540
DF15-02	90.691	BG4067	27/34	27.59 ± 1.21	14 ± 2	0.09 ± 0.01	2.55 ± 0.01	11.50 ± 0.01	0.91 ± 0.01	33 ± 3	0.199 ± 0.020	2.73 ± 0.12	10,100 ± 695
DF16-03	90.579	BG4074	36/50	23.88 ± 1.36	11 ± 1	0.05 ± 0.01	2.38 ± 0.01	11.15 ± 0.01	0.90 ± 0.01	33 ± 3	0.197 ± 0.020	2.30 ± 0.11	10,375 ± 740
DF15-04	90.504	BG4075	34/35	31.25 ± 1.14	9 ± 1	0.10 ± 0.01	2.57 ± 0.01	11.30 ± 0.01	0.91 ± 0.01	33 ± 3	0.195 ± 0.019	2.83 ± 0.13	11,060 ± 735
DF15-05	90.461	BG4068	31/35	35.08 ± 1.36	11 ± 2	0.09 ± 0.01	2.52 ± 0.01	11.50 ± 0.01	0.91 ± 0.01	33 ± 3	0.194± 0.019	2.71 ± 0.13	12,940 ± 855
DF15-06	90.405	BG4019	24/33	39.90 ± 1.22	5 ± 1	0.09 ± 0.01	2.74 ± 0.01	12.85 ± 0.01	0.94 ± 0.01	36 ± 3	0.193 ± 0.019	2.93 ± 0.12	13,620 ± 880
DF15-07	90.360	BG4017	34/35	37.54 ± 1.27	5 ± 1	0.09 ± 0.01	2.53 ± 0.01	11.70 ± 0.01	0.95 ± 0.01	36 ± 3	0.192 ± 0.019	2.69 ± 0.13	13,960 ± 965
DF15-08	90.334	BG4018	33/35	44.98 ± 1.64	12 ± 2	0.09 ± 0.01	2.91± 0.01	12.35 ± 0.01	0.96 ± 0.01	36 ± 3	0.191 ± 0.019	2.95 ± 0.14	15,265 ± 1000
DF15-09	90.270	BG4069	34/35	44.56 ± 1.60	8 ± 1	0.09 ± 0.01	2.76 ± 0.01	12.60 ± 0.01	0.94 ± 0.01	36 ± 3	0.190 ± 0.019	2.83 ± 0.13	15,725 ± 1030
DF15-10	90.218	BG4076	33/35	53.46 ± 1.69	7 ± 1	0.08 ± 0.01	2.74 ± 0.01	12.85 ± 0.01	0.88 ± 0.01	36 ± 3	0.189 ± 0.019	2.72 ± 0.13	19,680 ± 1320
DF15-11	90.177	BG4077	34/35	56.65 ± 1.87	8 ± 1	0.09 ± 0.01	2.78 ± 0.01	12.05 ± 0.01	0.91 ± 0.01	36 ± 3	0.188 ± 0.019	2.80 ± 0.13	20,250 ± 1340
DF15-12	90.119	BG4078	35/35	57.32 ± 1.92	5 ± 1	0.07 ± 0.01	2.69 ± 0.01	11.70 ± 0.01	0.86 ± 0.01	36 ± 3	0.187 ± 0.019	2.50 ± 0.12	22,950 ± 1445
DF15-13	90.066	BG4079	34/35	61.00 ± 2.40	13 ± 1	0.09 ± 0.01	2.60 ± 0.01	10.85 ± 0.01	0.81 ± 0.01	36 ± 3	0.186 ± 0.019	2.53 ± 0.12	24,145 ± 1635
DF15-14	90.212	BG3993	30/30	48.07 ± 1.70	2 ± 1	0.07 ± 0.01	2.66± 0.01	11.05 ± 0.01	0.86 ± 0.01	38 ± 3	0.188 ± 0.019	2.43 ± 0.12	19,750 ± 1245
DF15-15	90.247	BG3994	28/30	47.25 ± 1.57	3 ± 1	0.07 ± 0.01	2.64 ± 0.01	11.50 ± 0.01	0.83 ± 0.01	38 ± 3	0.189 ± 0.019	2.40 ± 0.12	19,650 ± 1230
DF15-16	90.312	BG3995	30/30	35.50 ± 1.16	3 ± 1	0.04 ± 0.01	2.66 ± 0.01	12.35 ± 0.01	0.94 ± 0.01	36 ± 3	0.190 ± 0.019	2.36 ± 0.11	15,020 ± 1010
DF16-01	90.644	BG4338	35/35	25.70 ± 0.96	7 ± 1	0.07 ± 0.01	3.16 ± 0.01	13.35 ± 0.01	1.08 ± 0.01	30 ± 3	0.220 ± 0.022	2.99 ± 0.15	8655 ± 550
DF16-02	90.594	BG4339	35/35	26.33 ± 1.04	10 ± 1	0.07 ± 0.01	2.54 ± 0.01	11.55 ± 0.01	0.88 ± 0.01	30 ± 3	0.210 ± 0.021	2.61 ± 0.13	10,095 ± 655
DF16-03	90.543	BG4340	34/35	27.88 ± 1.07	9 ± 1	0.08 ± 0.01	2.52 ± 0.01	11.40 ± 0.01	0.90 ± 0.01	30 ± 3	0.210 ± 0.021	2.69 ± 0.13	10,360 ± 705
DF16-04	90.492	BG4341	35/35	28.18 ± 1.08	8 ± 1	0.07 ± 0.01	2.63 ± 0.01	11.55 ± 0.01	0.95 ± 0.01	33 ± 3	0.205 ± 0.020	2.61 ± 0.13	10,830 ± 695
DF16-05	90.457	BG4207	33/34	22.78 ± 1.00	35 ± 3	0.06 ± 0.01	2.49 ± 0.01	9.54 ± 0.01	0.74 ± 0.01	33 ± 3	0.200 ± 0.020	2.16 ± 0.11	10,530 ± 750
DF16-06	90.434	BG4206	33/35	27.17 ± 0.65	7 ± 1	0.05 ± 0.01	2.90 ± 0.01	11.65 ± 0.01	0.96 ± 0.01	33 ± 3	0.198 ± 0.020	2.52 ± 0.13	10,785 ± 715
DF16-07	90.393	BG4208	46/50	27.98 ± 0.72	7 ± 1	0.07 ± 0.01	3.17 ± 0.01	9.01 ± 0.01	0.62 ± 0.01	33 ± 3	0.197 ± 0.020	2.30 ± 0.12	12,170 ± 820
DF16-08	90.360	BG4209	34/35	35.57 ± 0.73	12 ± 2	0.07 ± 0.01	3.31 ± 0.01	12.05 ± 0.01	0.93 ± 0.01	33 ± 3	0.196 ± 0.020	2.83 ± 0.14	12,560 ± 830
DF16-09	90.330	BG4218	34/35	33.07 ± 1.17	8 ± 1	0.08 ± 0.01	2.57 ± 0.01	10.90 ± 0.01	0.94 ± 0.01	36 ± 3	0.195 ± 0.020	2.54 ± 0.13	13,020 ± 870
DF16-10	90.307	BG4219	33/50	31.19 ± 1.26	18 ± 2	0.06 ± 0.01	2.62 ± 0.01	10.90 ± 0.01	0.95 ± 0.01	36 ± 3	0.194 ± 0.019	2.40 ± 0.12	13,010 ± 905
DF16-11	90.272	BG4220	36/50	29.93 ± 1.03	16 ± 2	0.05 ± 0.01	2.71 ± 0.01	10.05 ± 0.01	0.91 ± 0.01	38 ± 3	0.194 ± 0.019	2.20 ± 0.11	13,595 ± 930
DF16-12	90.245	BG4234	35/35	32.70 ± 0.81	8 ± 1	0.05 ± 0.01	2.70 ± 0.01	11.00 ± 0.01	0.83 ± 0.01	38 ± 3	0.193 ± 0.019	2.21 ± 0.12	14,790 ± 985
DF16-13	90.240	BG4235	34/35	32.33 ± 0.71	3 ± 1	0.05 ± 0.01	2.60 ± 0.01	10.85 ± 0.01	0.81 ± 0.01	38 ± 3	0.193 ± 0.019	2.16 ± 0.12	14,965 ± 985
DF16-14	90.217	BG4236	33/34	34.70 ± 0.82	8 ± 1	0.05 ± 0.01	2.66 ± 0.01	11.05 ± 0.01	0.90 ± 0.01	38 ± 3	0.192 ± 0.019	2.25 ± 0.12	15,400 ± 1015
DF16-15	90.186	BG4238	33/35	39.01 ± 0.87	6 ± 1	0.05 ± 0.01	2.90 ± 0.01	12.75 ± 0.01	1.01 ± 0.01	38 ± 3	0.191 ± 0.019	2.52 ± 0.13	15,500 ± 1020
DF16-16	90.154	BG4239	35/35	41.14 ± 1.11	11 ± 1	0.05 ± 0.01	2.74 ± 0.01	12.30 ± 0.01	1.05 ± 0.01	38 ± 3	0.190 ± 0.019	2.47 ± 0.13	16,650 ± 1110

†Aliquots used in equivalent dose calculations versus original aliquots measured.

‡Equivalent dose calculated on a pure quartz fraction and analyzed under blue-light excitation (470 ± 20 nm) by single aliquot regeneration protocols (*36, 37*). The central age model of Galbraith et al. (*41*) was used to calculate equivalent dose values with overdispersion values < 20%. One sample, DF16-05 (BG4207) yielded overdispersion of 35% and thus the Finite Mixture Model was used to calculate an equivalent dose (*48*).

§Values reflect precision beyond instrumental errors; values of ≤ 20% (at 1sigma limit) indicate low dispersion in equivalent dose values and an unimodal distribution.

‖U, Th and K content analyzed by inductively-coupled plasma-mass spectrometry analyzed by Activation Laboratory LTD, Ontario, Canada; U content includes Rb equivalent.

¶Cosmic dose rate calculated from parameters in Prescott and Hutton (*44*).

#Systematic and random errors calculated in a quadrature at one standard deviation. Datum year is AD 2010.

Table S2. Correlation of OSL ages with archaeological horizons.

Period	Bayesian modeled age (yr B.P.)	OSL age (yr B.P.)	Lab no.	Year
Late Prehistoric/Late Archaic/Middle Archaic				
	1000 ± 70	1000 ± 70	UIC2352	2008
Early Archaic				
	7295 ± 315	7030 ± 470	UIC2360s	2008
		7160 ± 470	UIC2360	2008
	7760 ± 370	8315 ± 540	BG4066	2015
	8260 ± 390	8160 ± 540	UIC2362	2008
	8370 ± 345	8070 ± 520	UIC2060	2007
		8490 ± 560	UIC2060Q	2007
	8950 ± 490	8655 ± 550	BG4338	2016
	9000 ± 380	9215 ± 620	UIC2061	2007
Late Paleoindian				
	9590 ± 370	9405 ± 610	UIC2363	2008
	9605 ± 400	9250 ± 600	UIC2052	2007
	9745 ± 420	10,095 ± 655	BG4339	2016
	9470 ± 380	10,100 ± 695	BG4067	2015
	10,245 ± 390	10,360 ± 705	BG4340	2016
	10,275 ± 385	9930 ± 640	UIC2364	2008
	10,375 ± 480	10,480 ± 675	UIC2051	2007
	10,465 ± 405	10,375 ± 740	BG4074	2015
	10,690 ± 370	10,830 ± 695	BG4341	2016
	10,965 ± 380	10,530 ± 750	BG4207	2016
	11,210 ± 405	10,785 ± 715	BG4206	2016
	11,505 ± 425	11,870 ± 760	UIC2365	2008
	11,575 ± 425	11,060 ± 735	BG4075	2015
	11,980 ± 555	12,690 ± 955	UIC2048	2007
Folsom and Clovis				
	11,980 ± 490	12,170 ± 820	BG4208	2016
	12,310 ± 435	12,940 ± 855	BG4068	2015
	12,455 ± 430	12,000 ± 770	UIC2366	2008
		12,100 ± 860	UIC2366A	2008
	12,500 ± 480	12,560 ± 830	BG4209	2016
	12,950 ± 480	13,020 ± 870	BG4218	2016
	13,090 ± 465	12,240 ± 800	UIC2045	2007
		12,925 ± 845	UIC2045Q	2007
	13,590 ± 720	13,090 ± 830	UIC2059	2007
		13,780 ± 885	UIC2059Q	2007
Boundary date				
	13,275 ± 500	13,010 ± 905	BG4219	2016
	13,565 ± 465	14,070 ± 910	UIC2354	2008
	13,625 ± 455	13,620 ± 880	BG4019	2015
	14,040 ± 510	14,350 ± 910	UIC2046	2007
Pre-Clovis				
	13,920 ± 540	13,595 ± 930	BG4220	2016
	14,235 ± 375	14,080 ± 920	UIC2367	2008
	14,270 ± 365	13,960 ± 965	BG4017	2015
	14,315 ± 360	14,370 ± 930	UIC2369	2008
	14,395 ± 495	15,270 ± 960	UIC2047	2007
	14,475 ± 365	14,000 ± 890	UIC2350	2008
		14,480 ± 920	UIC2350Q	2008
		14,580 ± 1030	UIC2350S	2008

Table S2 (cont.)

Period	Bayesian modeled age (yr B.P.)	OSL age (yr B.P.)	Lab no.	Year
	14,565 ± 505	14,790 ± 985	BG4234	2016
	14,665 ± 500	14,965 ± 985	BG4235	2016
	14,865 ± 435	15,265 ± 1000	BG4018	2015
	14,980 ± 445	15,730 ± 1010	UIC2359	2008
	15,035 ± 530	15,400 ± 1015	BG4236	2016
	15,135 ± 470	15,210 ± 960	UIC2043	2007
	15,190 ± 465	15,020 ± 1010	BG3995	2015
	15,415 ± 500	14,710 ± 940	UIC2356	2008
	15,470 ± 585	15,500 ± 1020	BG4238	2016
	15,590 ± 455	15,800 ± 1080	BG2044Q	2007
		16,400 ± 1040	UIC2044	2007
	15,965 ± 730	16,650 ± 1110	BG4239	2016
	16,235 ± 590	15,725 ± 1030	BG4069	2015
	16,400 ± 590	16,515 ± 1075	UIC2355	2008
Boundary date				
	15,950 ± 490	16,170 ± 1030	UIC2062	2007
	15,960 ± 495	15,110 ± 960	UIC2183	2007
	16,740 ± 660	16,270 ± 1040	UIC-2553	2008
	17,155 ± 820	17,530 ± 1140	UIC2368	2008
Pre-Occupation Floodplain deposits				
	18,475 ± 880	19,650 ± 1230	BG3994	2015
	19,410 ± 650	19,680 ± 1320	BG4076	2015
	19,515 ± 630	18,930 ± 1210	UIC2348	2008
	19,590 ± 630	19,750 ± 1245	BG3993	2015
	20,610 ± 685	20,250 ± 1340	BG4077	2015
		20,490 ± 1305	UIC2370Q	2008
	20,610 ± 685	20,565 ± 1325	UIC2370	2008
	21,240 ± 1035	20,330 ± 1320	UIC2058	2007
	22,380 ± 810	22,710 ± 1450	UIC2357	2008
		23,150 ± 1600	UIC2357S	2008
	23,115 ± 835	22,950 ± 1445	BG4078	2015
	23,735 ± 1000	24,420 ± 1580	UIC2057	2007
	24,160 ± 870	25,185 ± 1640	UIC2358	2008
	24,565 ± 890	24,145 ± 1635	BG4079	2015
	26,020 ± 1035	26,090 ± 1670	UIC2351	2008
		27,650 ± 1800	UIC2351Q	2008

Table S3. Clovis, Folsom, and Buttermilk Creek Complex Bifaces.

AM#	Max-width (mm)	Max-length (mm)	Max-thickness (mm)	Portion	Edge grinding	#over-shot	#over-face	Cross-section[†]	Elevation[‡]	Notes
12-13 ka Bifaces[§]										
Folsom points and preforms										
3069-6	21.2	27.2	3.9	distal	no			I	90.455	point
9717-43	17.7	31.5	2.8	proximal	no			I	90.449	preform - fluting failure
4525-1	2.2	21.9	4.5	distal	no			I	90.438	preform - fluting failure
Clovis points and preforms										
5784-8	27.4	38.8	7.5	distal		0	2	BC	90.484	point
4871-6	24.5	40.5	7.5	distal				BC	90.478	point
4447-1	21	17.4	4.7	midsection	yes			BC	90.468-90.435[5]	point- flute term. scars, both faces
9731-7	26.6	35.1	7.5	proximal		0	4	PC	90.45	preform - base bevel prep. for fluting
3138-4	15.5	25	6.1	distal				BC	90.425	point
9743-21	13	44.1	7.4	lateral		0	0	I	90.401	preform - fluting failure; isolated platform
4581-7	30.1	45.6	6.6	midsection				BC	90.4	point
12018-1	35	23	6.3	proximal	yes			PC	90.346	Point - concave base
12014-20	20.6	17.8	6.4	distal				BC	90.339	point
Clovis Bifaces										
8122-1	39	59.3	10.8	distal		2	5	PC	90.521	
6093-5	35.4	43.1	11.1	proximal		1	1	PC	90.512	end thinning both faces
4377-12	32.9	36.7	7.3	distal		0	4	PC	90.494	
4377-1	35.1	42.3	7.3	proximal		2	3	PC	90.481	
4449-4	52.2	38.6	11.4	midsection		0	1	BC	90.464	
9706-22	33.2	9.7	9.6	midsection		0	2	BC	90.456	
11851-9	39.9	48	9.2	proximal		0	2	PC	90.441	beveled base
5842-7	44.3	60.5	11	distal		1	5	PC	90.436	
4551-4	34.1	50.8	9.5	proximal		2	3	PC	90.432	
3183-1	36.5	52.1	10.1	proximal		0	3	PC	90.426	
3016-8	44.4	22.3	7.4	midsection		0	1	PC	90.412	
6225-13	32.4	41.6	8.3	distal		0	5	PC	90.403	
11948-1	27.4	32.2	8.2	distal		1	4	PC	90.4	
12010-1	43.6	58.8	9.5	distal		0	0	PC	90.355	
12262-19	41.1	69.7	9.1	distal		0	5	BC	90.347	
13-16 ka Bifaces[‖]										
Triangular Lanceolate Point										
9811-1	23	54	8.2	proximal	yes	0	4	PC	90.363	blade beveled
Lanceolate Stemmed Point										
8286-16	33.1	45.2	10.3	proximal		0	3	PC	90.385	expands from base
4668-6	28.2	36.1	6.5	distal		0	0	PC	90.384	slight alternate bevel
6233-1	20	28	6.5	proximal	yes	0	1	PC	90.36	blade beveled

Table S3 (cont.)

AM#	Max-width (mm)	Max-length (mm)	Max thickness (mm)	Portion	Edge grinding	#over-shot	#over-face	Cross-section[†]	Elevation[‡]	Notes
4819-7	25.3	30.9	81.6	midsection		0	1	PC	90.336	blade alternate bevel
12017-1	26	23.5	7	proximal	yes	0	0	PC	90.3	blade beveled
8380-3	11	14	5	distal		0	0	I	90.275-90.25[5]	blade alternate bevel
9875-2	20	53.5	7	complete	yes	0	0	PC	90.269	blade alternate bevel
12029-2	13.5	9	6.2	midsection		0	0	I	90.251	blade alternate bevel
12271-1	25	15	6	midsection	yes	0	4	PC	90.213	blade alternate bevel
12170-1	16.5	34.5	7.5	distal		0	0	BC	90.203	blade alternate bevel
12274-13	19	28	4.5	distal		0	2	PC	90.181	
Bifaces										
8264-1	35.5	64.3	11.5	lateral		0	0	PC	90.387	
8256-2	46.4	21.3	10.8	lateral		0	1	PC	90.367	
6223-3	27.7	29	8.7	proximal		0	0	PC	90.365	
6273-6	30	44.8	8.7	complete		1	0	PC	90.356	modified into end scraper
9855-1	43	75.4	10.7	distal		2	5	PC	90.336	
4777-2	18.4	59.6	7.3	lateral/proximal		0	0	PC	90.33	
6215-6	21.5	30.0	3.9	distal		0	1	PC	90.315	
9821-3	26.7	38.8	4.5	lateral		0	0	PC	90.313	bend-break tool
3277-1	47.9	50.7	14.8	distal		0	2	PC	90.306	
5965-2	26.9	37.8	8.5	lateral		0	0	PC	90.275	modified into bend-break tool
8408-1	24.9	43.9	5.9	lateral		0	0	PC	90.253	
12125-7	24.7	47.4	7.5	distal		0	1	PC	90.241	utilized broken edge
12085-1	54.3	55.3	12	midsection		0	1	PC	90.225	

[†]PC=Plano-convex; BC=Bi-convex; I=Indeterminate

[‡]meters above arbitrary datum

[§]Included here are bifaces with identifiable faking patterns. Not shown are 23 small/fragmentary bifaces, and 3 bifacial tools

[‖]Included here are bifaces with identifiable faking patterns. Not shown are 22 small/fragmentary bifaces